Apatite (U-Th)/He thermochronology and Re-Os ages in the Altar region, Central Andes (31°30'S), Main Cordillera of San Juan, Argentina: Implications of rapid exhumation in the porphyry Cu (Au) metal endowment and regional tectonics

Laura MAYDAGÁN[1-2]*, Massimiliano ZATTIN[3], Constantino MPODOZIS[4], David SELBY[5,6], Marta FRANCHINI[1-7], Luis DIMIERI[2]

[1] CONICET, Centro Patagónico de Estudios Metalogenéticos

[2]INGEOSUR-CONICET, Departamento de Geología, Universidad Nacional del Sur, San Juan 670, 8000 Bahía Blanca, Argentina

[3]Department of Geosciences, University of Padua, Via G. Gradenigo 6, Padova 35131, Italy

[4]Antofagasta Minerals, Apoquindo 4001, Piso 18, Santiago, Chile

[5]Department of Earth Sciences, University of Durham, Durham, DH1 3LE, UK

[6]State Key Laboratory of Geological Processes and Mineral Resources, School of Earth Resources, China University of Geosciences, Wuhan, China

[7]Departamento de Geología y Petróleo, Facultad de Ingeniería, Universidad Nacional del Comahue, Buenos Aires 1400, 8300 Neuquén, Argentina

*Corresponding author: lauramaydagan@yahoo.com.ar

Abstract

Altar is a large porphyry Cu (Au) deposit located in the Main Cordillera of Argentina, 20 km to the north of the giant Los Pelambres-El Pachón porphyry copper cluster, at the southern portion of the Pampean flat-slab segment of the Andes. Although this region hosts telescoped porphyry-epithermal deposits, the precise temporal relationship between porphyry emplacement, mineralization, cooling, and regional orogenic uplift are still poorly understood.

New Re-Os molybdenite ages indicate that Altar orebodies are associated with two magmatic hydrothermal centers: Altar East (11.16 ± 0.06 Ma) and Altar Central (10.38 ± 0.05 Ma) formed at temporally distinct periods. New (U-Th)/He ages from the Early Permian and Late Eocene plutons, and the Middle Miocene subvolcanic stocks associated with Cu-Au mineralization of the Altar region reflect a rapid cooling pulse during the Middle Miocene (15.02 to 10.66 Ma) coeval with a major phase of tectonic shortening and regional uplift.

The main pulse of rapid cooling and related tectonic uplift in the Altar region was synchronous with the formation of the hydrothermal systems and resulted in an increased focused metal endowment (Au-Cu grades) due to the telescoping of epithermal mineralization over the rapidly uplifted porphyry system. This 11-10 Ma tectonically triggered exhumation event coincides with the collision of the E-trending segment of the Juan Fernández Ridge with the Peru-Chile trench, at this latitude. Collision and ensuing ridge subduction may have driven a localized pulse of rapid cooling and exhumation of the Main Cordillera, that has not been well documented to the north or south of the Altar-Los Pelambres region.

Keywords: U-Th/He in apatite, Andes, Miocene, Re-Os in molybdenite, Exhumation, Argentina

Introduction

Altar is a large porphyry Cu (Au) deposit with associated high sulfidation epithermal veins (measured and indicated resources of 2 Gt at 0.34 % copper and 0.1 g/t gold, Aldebaran Resources 2018), located in the Cordillera Principal of San Juan Province, Argentina, near the Argentina-Chile border. The deposit occurs at the southern portion of the modern Pampean flat-slab segment (Cahill and Isacks 1992; Kay and Mpodozis 2002; Anderson et al. 2007; Haddon and Porter 2018, Fig. 1) and forms part of the southern Central Andes Miocene-Pliocene porphyry copper belt that, in Chile, hosts three of the largest copper deposits in the world (El Teniente: 75 Mt Cu; Río Blanco-Los Bronces: 204 Mt Cu, Los Pelambres-El Pachón: 21 Mt Cu; Cooke et al. 2005; Sillitoe and Perelló 2005; Irarrazaval et al. 2010, Fig. 2). Numerous Cu (Au) prospects with high mining potential have been recently discovered in the area, some exhibiting telescoped porphyry type and high sulfidation epithermal systems. These telescoped systems are interpreted to reflect synmineral erosion, progressive paleosurface lowering and alteration-mineralization overlapping as result of compressive deformation and uplift (e.g., Sillitoe 1994; Sillitoe et al. 2019).

The Altar deposit represents an environment that transitions from the basal roots of a high sulfidation epithermal lithocap to a sub-volcanic porphyry copper environment at depth. The deposit is described as telescoped because of the close spatial distance between the porphyry and the high sulfidation alteration systems (Aldebaran Resources 2018). Metallic mineralization at the Altar Central orebody occurred through successive stages of vein formation: 1) quartz ± chalcopyrite ± pyrite veins (A veins), and 2) quartz ± molybdenite veins (B veins), both formed during early potassic alteration at high temperature and pressures, and 3) late stage veins rich in Cu sulfides and sulfosalts (E veins) that formed at low temperatures equivalent or transitional to the epithermal environment, and cross-cut the early veins (Maydagán et al. 2015). The epithermal veins are considered to be slightly younger than the porphyry veins implying that the hydrothermal system would have developed in an active tectonic environment.

In this study we present new Re-Os molybdenite data to better constrain the timing of Altar mineralization, and new apatite (U-Th)/He data in order to investigate the low-temperature

cooling history of igneous and sedimentary rocks of the region. We analyze the causes of cooling and discuss whether the cooling events related to the tectonic pulses could affect the presence and grade of porphyry-epithermal mineral deposits. We compare our results with the tectonic/uplift history of the Coastal, Main and Frontal Cordilleras at this latitude, and with previous studies in other areas of the modern Pampean flat-slab region.

Tectonic Setting

The Altar deposit is located in the present-day amagmatic Pampean flat-slab segment of the central Argentina and Chile, which hosts two of the three largest known porphyry copper-molybdenum deposits of Central Chile: Río Blanco-Los Bronces and Los Pelambres-El Pachón, Cooke et al. 2005; Sillitoe and Perelló 2005; Irarrazaval et al. 2010; Fig. 1). This metallogenic belt was constructed atop the Chilenia Terrane, a microcontinental block accreted to the Gondwana margin in the Devonian (Ramos et al. 1986) that was later the site of subduction-related arc-magmatism during the Pennsylvanian to early Permian (Mpodozis and Kay 1992), rifting and extension-related magmatism during the Middle Permian to Triassic (Sato et al. 2015), marine sedimentation in a backarc setting (Neuquén Basin) during the Jurassic-Early Cretaceous (Cristallini and Ramos 2000), and subduction-related calc-alkaline volcanism and associated plutonism during the Cretaceous through the Cenozoic (Mpodozis and Ramos 1989). During the Oligocene and Early Miocene, thick volcano-sedimentary sequences accumulated in an extensional volcano-tectonic basin or intra-arc depression (Abanico/Coya Machalí Basin, Jordan et al. 2001; Charrier et al. 2002, 2005). Compressional deformation and basin collapse began in the Early Miocene at ca. 20-18 Ma, coinciding with the initiation of the oceanic Nazca slab shallowing (Kay and Mpodozis 2002).

Geology of the Los Pelambres-Altar region (31°-32°S)

The geology of the Altar-Los Pelambres region is characterized by four structural domains that show different stratigraphy and structural style and are bounded by N-trending, high-angle reverse faults.

104 The easternmost Domain 1, encompasses a westward-tilted block including granites and
105 silicic volcanic rocks assigned to the Permo-Triassic Choiyoi Group (Alvarez 1996; Cristallini
106 and Ramos 2000) that form the highest peaks of the Cordillera Santa Cruz (Fig. 2). This block is
107 thrust toward the east, on top of the major high angle, west dipping reverse, Santa Cruz Fault,
108 over Miocene synorogenic (<18 Ma) red conglomerate and sandstone sequences (Cristallini and
109 Ramos 2000). To the west the Choiyoi Group is unconformably covered by Late Triassic rift
110 (ca. 200 Ma) deposits (Rancho de Lata Formation, Alvarez 1996; Mackaman-Lofland et al.
111 2019) and a thin sequence of Jurassic to Cretaceous marine and continental sedimentary strata
112 that include the northernmost known outcrops of the Neuquén backarc basin infill (Alvarez
113 1996; Cristallini and Ramos 2000). These Mesozoic sedimentary rocks are, in turn,
114 unconformably covered by continental volcaniclastic conglomerate and breccia, rhyolitic tuff,
115 and pyroxene-hornblende bearing andesite and dacite, grouped as the Mondaca Strata, which
116 yielded LA-ICPMS U-Pb zircon ages between 22.1 ± 0.4 and 21.6 ± 0.4 Ma (Mpodozis et al.
117 2009, Fig. 2). To the south, 20°-30°W dipping rocks of this unit are covered, in angular
118 unconformity, by gently dipping to subhorizontal Lower Miocene volcanic rocks with LA-
119 ICPMS U-Pb ages between 20 and 14 Ma (Laguna del Pelado and Yunque volcanic complexes,
120 Mpodozis et al. 2009, Fig. 2), which provides evidence of a regional compressive deformation
121 event at ~20 Ma. Middle to Late Miocene intrusions in this domain are linked to porphyry type
122 deposits (e.g., El Yunque, Fig. 2).
123 Domain 2 is bounded by another east-verging reverse fault (Mondaquita Fault) that brings
124 “basement” late Paleozoic-Triassic rocks on top of the Mondaca Strata and/or the Laguna del
125 Pelado Volcanic Complex (Fig. 2). The oldest rocks of this domain include small and isolated
126 outcrops of clastic metasedimentary rocks (Alfarcillo Metamorphic Complex, Musso et al.
127 2012) and undated silicic volcanic rocks intruded by Late Carboniferous to Early Permian
128 granitoids of the Pico Los Sapos batholith (Mpodozis et al. 1976) that includes 297 ± 4 Ma
129 tonalite (zircon LA-ICPMS U-Pb age, Maydagán 2012) and granite dated at 301.4 ± 2.3 Ma by
130 the same method (Musso et al. 2012). The Paleozoic rocks are capped, between Río Carnicería
131 and Río Pantanosa, by a sequence of around 500 m of rhyolitic lavas and pyroclastic rocks

which yielded a Middle Triassic LA-ICPMS U-Pb zircon age (ca. 239 Ma, Mpodozis et al. 2009; Mpodozis 2016). The western area of Domain 2 is formed by regionally extensive outcrops of olivine-bearing basaltic to andesitic lava flows and rare felsic tuff of the Pachón Formation (Fernández et al. 1974; Lencinas and Tonel 1993) with U-Pb zircon ages between 22.7 ± 0.2 and 21.69 ± 0.26 Ma (Mpodozis et al. 2009; Perelló et al. 2012). Outcrops of the Pachón Formation are bounded to the east by the Pachón Fault (Fig. 2), a west dipping, partly inverted normal fault, that brings the volcanic rocks in contact with Late Paleozoic to Middle Triassic rocks (Mpodozis et al. 2009).

Rocks belonging to the Pachón Formation host the late Miocene subvolcanic porphyry intrusions associated with the El Pachón (Fernández et al. 1974), Piuquenes and Altar porphyry copper systems (Fig. 2). At Altar they include a lower unit of basaltic andesite and porphyritic andesite-dacite lavas, andesitic-dacitic lapilli tuff, and pyroclastic breccia that grade upwards to a unit of compact and thick rhyolitic tuff (U-Pb zircon ages of 21.6 ± 1.2 Ma and 20.8 ± 0.3 Ma, Maydagán et al. 2011; Maydagán 2012). Both the Pachón Formation and the Mondaca Strata are, in part, equivalent to the regionally extensive volcanic Abanico/Coya-Machalí formations that form the bulk of the main Cordillera of Central Chile (33°–36ºS, Aguirre 1960; Klohn 1960; Thiele 1980; Charrier et al. 2002; Piquer et al. 2017).

Domain 3 is a narrow 5-km-wide, N-trending ribbon of strongly deformed volcanic and sedimentary rocks straddling the Argentina-Chile border and bounded to the east by the high angle, reverse, E-verging Los Pelambres-Pantanosa Fault System, and to the west by the W-verging Totoral-Tres Quebradas faults (Fig. 2). Near the Los Pelambres deposit, Domain 3 comprises a sequence of andesitic to basaltic lava flows, tuff and local lacustrine ostracods-bearing limestone (Los Pelambres Formation), first described by Rivano and Sepúlveda (1991) who attributed this unit to the early Cretaceous. Several LA-ICPMS U-Pb zircon ages ranging from 33.4 to 18.0 Ma confirm, however, its Early Oligocene to Early Miocene age (Mpodozis et al. 2009; Perelló et al. 2012). This unit is intensely deformed as indicated by vertical and overturned strata, anastomosing, thrust-bounded tectonic lenses, and widespread mesoscale, sub-isoclinal folds (Mpodozis et al. 2009; Mpodozis 2016). The high strain Domain 3 can be

160 traced northward into the Altar region, bordered by the La Pantanosa and Tres Quebradas faults
161 where a sequence of continental red beds and andesitic to basaltic lavas, not yet dated, but likely
162 of Cretaceous age (Fig. 2), are intruded by the Late Eocene del Medio Pluton (Mpodozis 2016,
163 Fig. 3).

164 Middle to Late Miocene intrusions (14 - 8 Ma) related to the mineralized systems of Los
165 Pelambres, Pachón, Piuquenes and Altar, representing the last episodes of magmatic activity in
166 the region, outcrop in Domains 2 and 3 (Fig. 2). In the Los Pelambres porphyry deposit, the
167 post-kinematic and pre-mineral Los Pelambres stock, that was emplaced along the trace of Los
168 Pelambres Fault at the boundary between domains 2 and 3 (Fig. 2), yielded LA-ICPMS U-Pb
169 ages of 13.92 ± 0.15 and 13.00 ± 0.7 Ma (Bertens et al. 2003, 2006; Perelló et al. 2012). The
170 Los Pelambres-Frontera cluster of Cu-Mo mineralized porphyries, that intrude both the
171 precursor stock and the Pachón Formation of Domain 2, have LA-ICPMS U-Pb zircon
172 crystallization ages between 12.3 and 10.5 Ma (Perelló et al. 2012). By comparison, the
173 intrusive suite hosting the majority of Cu-Au mineralization at Altar comprises a series of
174 porphyritic intrusions, dykes and magmatic-hydrothermal breccias emplaced in the Pachón
175 Formation, but no early large precursor stock as in Los Pelambres has been found (Maydagán et
176 al. 2014, Fig. 3).

177 Altar hosts three main porphyry copper-gold mineralization centers: Altar East, Altar
178 Central and the recently discovered Quebrada de la Mina-Radio, 3 km to the west of Altar
179 Central. Zircon LA-ICPMS U-Pb ages from the Altar East and Altar Central orebodies indicate
180 the occurrence of four discrete intrusive events over a period of ca. 3 m.y. The intrusions
181 comprise a pre-mineralization porphyry (porphyry 1, 11.75 ± 0.24 Ma), three mineralized
182 porphyries related to hydrothermal breccias (porphyry 2, 11.62 ± 0.21 and 11.68 ± 0.27 Ma;
183 porphyry 3, 11.13 ± 0.26 Ma; porphyry 4, 10.35 ± 0.32 Ma), and two post-mineralization
184 intrusions along with a post-mineralization intrusive breccia (8.9 ± 0.4 Ma, Maydagán et al.
185 2011, 2014, Fig. 3). Altar is noteworthy for having relatively higher gold grades associated with
186 copper mineralization, at an average Au/Cu ratio of 0.14×10^{-4} for the Altar Central orebody

(Zwahlen et al. 2014), compared to the nearby giant Chilean deposits such as Los Bronces and Los Pelambres (Mutschler et al. 2010).

The westernmost Domain 4 in Chile, west of the Totoral-González and Tres Quebradas faults is, by contrast, characterized by a >2-km thick, unfolded, gently E-dipping sequence of Middle to Late Cretaceous sedimentary and volcanic strata (from base to top: Quebrada Marquesa Formation, Salamanca Formation and Almendrillo Strata) which, at this latitude, form the youngest Mesozoic stratified sequences of the Chilean Coastal Range (Rivano and Sepúlveda 1991; Mpodozis et al. 2009; Bergoeing 2016, Fig. 2). North of Los Pelambres, an Early Paleocene volcanic sequence rests on top of the Almendrillo Strata (75-70 Ma) while, to the south, the Cretaceous rocks are covered, through a remarkable angular unconformity by a Late Oligocene to Early Miocene volcanic sequence (Río Chicharra Strata, Fig. 2). Late Cretaceous, Paleocene, Eocene, Oligocene and Early to Middle Miocene plutons and stocks, of generally intermediate composition, intrude the volcanic and volcano-sedimentary sequences of Domain 4 (Fig. 2).

Methodology

A suite of samples was collected from the Altar region to carry out geochronological analysis by Re-Os in molybdenite and (U-Th)/He in apatite (ESM 1).

Two molybdenite samples, obtained from the drill-holes of the Altar Central and Altar East deposits, were analyzed in the Source Rock and Sulfide Geochemistry and Geochronology, and Arthur Holmes Laboratories at University of Durham (United Kingdom) to establish the Re-Os age of molybdenite mineralization (ESM 1). Samples of B veins rich in molybdenite were selected from the Altar East deposit (drill hole ALD-178, depth 153 m) and the Altar Central deposit (drill hole ALD-68, depth 440 m). Molybdenite separation was achieved through using traditional methods (crushing to 70 to 200 mesh, magnetic separation, heavy liquids and final hand picking to remove any impurities). An aliquant of the molybdenite separate (~20 mg) together with a known amount of tracer solution (^{185}Re + Os bearing a normal isotope composition) were placed into a carius tube and digested with 3mL HCl and

6mL HNO_3 at 220°C for 23 hrs. Osmium was isolated and purified using solvent extraction ($CHCL_3$) and microdistillation methods, with the resulting Re-bearing fraction purified using NaOH-Acetone solvent extraction and anion chromatography (Selby and Creaser 2004; Li et al. 2017). Although negligible in comparison to the Re and Os abundance in the molybdenite, the final Re-Os data are blank corrected. A full analytical protocol blank run parallel with the molybdenite analysis yields 3.2 pg Re and 0.8 pg Os, the latter possessing a $^{187}Os/^{188}Os$ composition of 0.21 ± 0.2. See Li et al. (2017) regarding data treatment, standards and reference materials.

Two samples for U-Th/He analysis were obtained from the Late Carboniferous-Early Permian tonalites of the Pico Los Sapos batholith (Samples A24 and A8, Fig. 3). One sample was obtained from the Late Eocene del Medio Pluton (Fig. 3). Two samples were taken from a volcanic-sedimentary unit (Chinchimoye sequence), considered to be of Miocene age that crops out north of Quebrada de la Mina-Radio deposit (A12 and A19), and six samples (A1, A2, A5, A16, A17, A22) were taken from the Middle-Late Miocene porphyry intrusions (Fig. 3).

The mineral separates of the apatite crystals for U-Th/He analysis was carried out in both the laboratories of the Universidad Nacional del Sur (Argentina) and the University of Padova (Italy). The (U-Th)/He single grain ages were obtained from selected apatite grains (euhedral shape, overall size greater than 60 μm and without inclusions) at the University of Arizona, Tucson (USA). Sphere equivalent radius, weight, and ejection factors were determined assuming a homogeneous distribution of U and Th in apatite (Gautheron and Tassan Got 2010; Gautheron et al. 2012). The apatite samples were placed in a niobium (Nb) basket and were heated twice using a diode laser at 1030 ±50°C for 5 minutes, allowing for total He degassing and to check the presence of He trapped in small inclusions (Fillon et al. 2013). After He extraction, the Nb baskets were placed into a single-use polypropylene vial. Apatite grains were dissolved for 3 h at 70°C in 50 μL HNO_3 5N solution containing a known content of ^{235}U, ^{230}Th, and ^{149}Sm, and additional 50 μL HNO_3 5N and then filled with 0.9 mL of ultrapure MQ water. The final solution was measured for U, Th, and Sm concentrations by quadrupole inductively coupled plasma (ICP)-quadrupole mass spectrometry. The analysis was calibrated using

external age standards, including Limberg Tuff and Durango apatites. The mean (U-Th)/He ages of the standards agree with published data (16.8 ± 1.1 Ma and 31.0 ± 1.0; McDowell et al. 2005; Kraml et al. 2006).

Results

Re-Os dates in molybdenite

Molybdenite from the Altar East deposit (drill hole ALD-178) contains 3546 ppm Re and 414 ppb ^{187}Os and yielded a Re-Os age of 11.16 ± 0.06 Ma, including analytical, tracer and decay constant uncertainties. In comparison, the molybdenite from the Altar Central deposit (drill hole ALD-68) has lower Re (1868 ppm) and ^{187}Os (203 ppb), with a younger Re-Os age of 10.38 ± 0.05 Ma (Table 1, Figs. 4 and 5a).

U-Th/He dates in apatite

All apatite U-Th-He analytical data and weighted mean (U-Th)/He ages are presented in Table 2 and ESM 1. The Early Permian tonalite of the Pico Los Sapos Batholith (samples A-8 and A-24, Figs. 3 and 5b-c) yielded single grain (U-Th)/He ages between 15.69 and 10.66 Ma, with mean (U-Th)/He ages of 14.3 ± 0.29 Ma (number of grains = 3) and 11.87 ± 0.15 Ma (n = 3), respectively (Fig. 5b). The sample from the Late Eocene Plutón del Medio (PDM18), that crops out in the west sector of the Altar District (Figs. 3 and 5b-c), yielded single grain (U-Th)/He ages between 15.02 and 12.98 Ma, with a mean (U-Th)/He age of 13.46 ± 0.17 Ma (n = 2).

The two samples from the Miocene red sandstone and conglomerate of the Chinchimoye Sequence (A12 and A19) yielded individual (U-Th)/He grain ages of 29.63, 27.58 and 6.15 Ma, and 55.57, 46.60 and 24.44 Ma, respectively. Sample A-19 yield two grains older than their proposed Miocene age (Figs. 3 and 5b).

The majority of the (U-Th)/He ages from the Middle to Late Miocene Altar subvolcanic stocks (70 %) range between 14.87 and 9.96 Ma (Figs. 3 and 5b-c). Sample A-1 from the Altar North porphyry intrusion gave (U-Th)/He ages between 12.99 and 11.53 Ma, with a mean (U-

Th)/He age of 12.18 ± 0.15 Ma. Sample A-2 (Altar North porphyry) exhibits (U-Th)/He ages older than the crystallization age of the intrusion (56.83 Ma, 30.92 Ma and 26.17 Ma, Table 2). Samples A-22 and A-5 from Altar East porphyry intrusions yielded (U-Th)/He ages between 14.87 and 9.96 Ma, and mean (U-Th)/He ages of 11.17 ± 0.4 Ma and 12.32 ± 0.26 Ma, respectively. Sample A-17 from a subvolcanic stock of Quebrada de la Mina deposit yielded (U-Th)/He ages between 14.87 and 12.8 Ma (mean (U-Th)/He age of 13.45 ± 0.27 Ma). Finally, one apatite crystal from sample A-16 yielded an (U-Th)/He age of 0.82 Ma ± 0.04 (Table 2).

Discussion

Ages of porphyry emplacement and mineralization

Metallic mineralization at the Altar Central orebody occurred through successive stages of vein formation: 1) quartz ± chalcopyrite ± pyrite veins (A veins), and 2) quartz ± molybdenite veins (B veins), both formed during early potassic alteration at high temperature and pressure, and 3) late stage veins rich in Cu sulfides and sulfosalts (E veins) that formed at low temperature equivalent or transitional to the epithermal environment (Maydagán et al. 2015). In the eastern sector of the Altar deposit, the roots of an epithermal lithocap are exposed, whereas in the central orebody, epithermal veins cross cut the porphyry A and B (Maydagán et al. 2015). Fluid inclusions studies have been interpreted to suggest temperatures of 540° to 510°C and pressures of 1,000 to 800 bars for the formation of stage 2 B veins, whereas stage 3 E veins formed, under hydrostatic conditions, from 280° to 250°C fluids at pressures of 150 to 20 bars (Cioldi 2009; Maydagán et al. 2015).

The two new Re-Os molybdenite dates are interpreted to define the absolute timing of stage 2 B vein mineralization in Altar East (11.16 ± 0.06 Ma, Table 1) and Altar Central (10.38 ± 0.05 Ma; Table 1) to be Middle Miocene. These ages are nominally different even when including full analytical and decay constant uncertainties (Table 1). As such, although only two ages, the Re-Os molybdenite data suggest that the Altar East and Altar Central deposits were associated with two magmatic hydrothermal centers, as suggested by Maydagán et al. (2014) that were active during two different time periods (Fig. 5a).

Altar East molybdenite (11.16 ± 0.06 Ma) formed a little after the intrusion of Porphyry 2 (11.62 ± 0.21 and 11.68 ± 0.27 Ma) and was contemporaneous, considering uncertainty, with the emplacement of Porphyry 3 (11.13 ± 0.26 Ma). In contrast, the Altar Central molybdenite B veins formed later (10.38 ± 0.05 Ma), at the same time or shortly after the emplacement of Porphyry 4 (10.35 ± 0.32 Ma). The Re-Os ages thus confirm that Altar Central is the youngest magmatic-hydrothermal system in the Altar district.

The mineralization events at Altar can be compared with those from Los Pelambres and El Pachón porphyry deposits, located ~25 km south (Fig. 2). Zircon U-Pb crystallization ages of the mineralized porphyries (12.3 to 10.5 Ma) together with the Re-Os molybdenite ages (11.8 to 10.1 Ma) in the Los Pelambres-Frontera system (Bertens et al. 2003, 2006; Perelló et al. 2012, Fig. 6a) are similar to those of the Altar porphyries and mineralization (Maydagán et al. 2014; this study). Available Re-Os molybdenite ages from El Pachón deposit are, however, younger (9.16 and 8.43 Ma, Bertens et al. 2006, Fig. 6a) and reflect the youngest mineralization event recognized in the Altar-Los Pelambres region (Figs. 2 and 6a).

Cooling and exhumation of the Altar district and nearby Los Pelambres-El Pachon deposits

The dispersion of the U-Th/He ages of the Chinchimoye volcanic-sedimentary sequence (samples A-12 and A-19) suggests, at a first glance, that these rocks were not buried sufficiently (<2 km, depth of the 60°C isotherm) to reset the U-Th/He system and that the dated apatite still retain, in part, an inherited pre-depositional signal (Fig. 5b). An alternative view for the range in single grain apatite ages is the effect of hydrothermal activity that may influence the thermochronological data sets. However, the sampled sites as well as the volcanic-sedimentary sequence show limited evidence of hydrothermal activity.

The conditions to reset thermochronology systems by late hydrothermal fluids require the fluids to be transported along steeply dipping faults, with a very narrow fracture zone, which results in developing a reset zone that is limited to not more than a few tens of meters around the fault (Luijendijk 2019). The majority of the samples analyzed in this contribution were

taken at distance of more than 1-2 km from faults (PDM18, A-12, A-19, A-1, A-2, A-5, A-8, A-24), thus there is no clear evidence to support this hypothesis.

The (U-Th)/He ages obtained in the Altar region, from the Early Permian Pico Los Sapos batholith (LA-ICPMS U-Pb zircon age of 297 Ma, Maydagán 2012) and the Late Eocene Plutón del Medio tonalite (LA-ICPMS U-Pb zircon age of 34.1 Ma, Mpodozis 2016), that range between 15.02 and 10.66 Ma (Table 2; Figs. 3 and 5b-c) reflect a cooling pulse during the Middle Miocene, both in the western sector and in the eastern sector of the Altar deposit. The (U-Th)/He ages of the Permian and Eocene intrusive rocks overlap with the (U-Th)/He dates obtained for the Altar porphyry intrusions (between 14.87 and 9.96 Ma), which also, considering uncertainties, are similar to the U-Pb porphyry crystallization ages (~11.9 - 10.3 Ma, Maydagán et al. 2011, 2014, 2017).

Porphyry deposits occur within magmatic belts worldwide and are spatially, temporally, and genetically related to hypabyssal porphyritic intrusions emplaced at depths between ~2 and 6 km (Seedorff et al. 2005; Sillitoe 2010). The intrusions and magma chambers linked to these deposits underwent volatile exsolution and produced a sequence of hydrothermal alteration from ~700° to 200°C (Seedorff et al. 2005; Sillitoe 2010).

The overlap of U-Pb, Re-Os and (U-Th)/He ages recognized in the Altar subvolcanic stocks, which indicate a very rapid cooling of the magmatic-hydrothermal system, is atypical of low temperature thermochronology studies on porphyry deposits, where there are generally two distinct cooling periods: magmatic-hydrothermal cooling after emplacement of the intrusion and exhumation cooling (e.g. McInnes et al. 2005; Leng et al. 2018). The overlap in the ages of this study can occur in two ways, 1) the porphyry intrusions are located at very low depths in the crust or 2) a tectonic exhumation event occurs immediately after the emplacement of the intrusion. An example of the first option is the Grasberg porphyry system (Indonesia) in which a depth of emplacement of ~0.8 km has been estimated for the intrusion (McInnes et al. 2005). As examples of rapid cooling linked to tectonic exhumation we can mention the Middle Eocene dacitic intrusions of the Centinela District (Atacama, Chile), with similar U-Pb and apatite

354 fission track (AFT) ages, that have been interpreted as intruded during the Incaic tectonic phase
355 (Sanchez et al. 2018).
356 The subvolcanic intrusions of the Altar porphyry deposit were emplaced at depths of 3.5-
357 5 km based on the following evidence: 1) amphibole phenocrysts from porphyry 1 (Altar East)
358 are estimated to have crystallized at 800 °C and pressures between 0.9 and 1.2 kbar that reflect
359 depths of ~4 km for pluton emplacement (Maydagán et al. 2014); 2) the early quartz veins have
360 fluid inclusions of intermediate density (Maydagán et al. 2015) that are abundant in samples,
361 1000 to 600 m below the present surface. The presence of irregular A veins and the fluid
362 inclusions that showed homogenization temperatures between 400° and 540° C reflect the
363 formation of the veins at lithostatic pressures (Fournier 1999). Exsolution of magmatic volatiles
364 from a crystallizing hydrous magma in the single-phase fluid stability region occur at pressures
365 higher than 1,000 bar (e.g., William Jones and Heinrich 2005) equivalent to depths of > 3.5 km
366 at lithostatic pressures and; 3) fluid inclusion studies on B-type veins have been interpreted to
367 indicate pressures of 1,000 to 800 bar which correspond to depths of 3.7 to 3 km under
368 lithostatic pressures. In contrast, the telescoping stage 3 epithermal E veins formed, under
369 hydrostatic conditions, from 280° to 250°C fluids at pressures of 20 to 150 bar that reflect
370 depths of <2 km (Cioldi 2009; Maydagán et al. 2015).
371 Considering the temporal data together with the available geological and metallogenetic
372 information of the Altar system, we interpret that the rapid cooling recognized in the Altar
373 intrusions reflects an exhumation pulse that occurred immediately after the emplacement of the
374 subvolcanic intrusion, and that the cooling and related exhumation was contemporaneous with
375 the hypogene mineralization stage of the hydrothermal system.
376 An alternative interpretation for the (U-Th)/He ages of the subvolcanic stocks sampled
377 close to the porphyry deposit (A-22, A-16, A-17, Fig. 4) would be that the ages indicate the
378 cessation of the hydrothermal activity (<75 °C). If we consider this hypothesis, it should be
379 noted that more than 50% of the apatite crystals from the subvolcanic stocks have (U-Th)/He
380 ages between 12-10 Ma, indicating that the hydrothermal activity of the porphyry and
381 epithermal systems (that are vertically spatial close and are superimposed) would have formed

382 in a short time interval. This provides indirect evidence of uplift, exhumation and erosion that
383 allowed the porphyry and epithermal systems to be superimposed in a short period of time.
384 Models and field examples of porphyry and lithocap systems in regions without telescoping
385 occur at a vertical distance of ~1 km such as the Valeriano lithocap and associated porphyry
386 copper-gold deposit in northern Chile (Sillitoe 2010; Sillitoe et al. 2016).
387 Given that (U-Th)/He ages refer to the timing of the closure temperature for He in apatite
388 at ~60–70 °C (Zeitler et al. 1987; Wolf et al. 1998; House et al. 1998; Farley 2002), the (U-
389 Th)/He ages reflect the time when the rocks pass through depths shallower than ~2-3 km. Thus,
390 the U-Pb and (U-Th)/He ages of the porphyry intrusions indicate that the temperature decreased
391 from magmatic crystallization at 800°C to 60–70°C in a very short period of time. Given that
392 the majority of the porphyry intrusions in the Altar deposit were emplaced at ~11.75 – 11.62 Ma
393 and the younger individual (U-Th)/He ages are ~10 Ma, the porphyry intrusions would have
394 been uplifted from its depth of formation at ~4 km to depths shallower than 3 km, and more
395 likely shallower than 2 km based on the epithermal characteristics at Altar Central, in a period
396 of <2 m.y., suggesting high exhumation rates of 0.5-1 km/myr. These exhumation rates are in
397 agreement with a more quantitative estimation (0.4 and 0.6 for a geothermal gradient of
398 30°C/km and 0.5 and 0.7 for a geothermal gradient of 20°C/km) derived by converting the
399 thermochronometric ages into exhumation rates (Willett and Brandon 2013), using the best
400 estimates of the present-day geothermal gradient (Collo et al. 2011; Stevens Goddard and
401 Carrapa 2018).
402 Lithocaps are large rock volumes, originally 1 to 2 km thick and up to tens of square
403 kilometers in areal extent, that normally constitute the upper parts of porphyry copper systems
404 (Sillitoe 1995). The eastern ridges that surround the Altar east orebody are cut by siliceous
405 ledges that crop out at the surface and have been interpreted to be the basal part of an advanced
406 argillic lithocap (Peregrine Metals Ltd. 2011). A sample of hypogene alunite corresponding to
407 the Altar East lithocap has been dated by Ar-Ar at 12 Ma (Maydagán 2012) reflecting an uplift
408 event after 12 Ma that produced the erosion of the epithermal lithocap and preserved only its

409 roots. The presence of the lithocap remnant would imply at least 1 km of erosion at Altar East
410 and > 1 km of erosion at Altar Central.
411 Further, the similarity of the (U-Th)/He ages at Altar with those of the Permian and
412 Eocene aged plutons indicate that this rapid uplift was not localized to the Altar porphyry-
413 epithermal system, but occurred at a regional scale during the Middle Miocene (14-10 Ma, Fig.
414 5c). Moreover, the (U-Th)/He zircon and (U-Th)/He ages (10.37 to 8.15 Ma; Bertens et al.
415 2006, Fig. 6b) recorded in the Los Pelambres deposit, slightly younger than Altar (U-Th)/He
416 ages and very close to the timing of porphyry mineralization (11.66 to 11.00 Ma), coupled with
417 a $^{40}Ar/^{39}Ar$ jarosite age (5.34 Ma; Bertens et al. 2006) for supergene alteration, indicate an
418 episode of rapid regional exhumation during the Middle Miocene.
419 The cooling and interpreted uplift event recorded by the (U-Th)/He ages of the Paleozoic
420 granitoids of the Pico Los Sapos Batholith (14.3 and 11.87 Ma, this study, Figs. 5b-c) coincide
421 with a < 14 Ma period of tectonic activity recorded on the Mondaquita Fault (boundary between
422 Domains 1 and 2, Fig. 2) by geological relationships (Mpodozis 2016). South of Río Carnicería,
423 the Mondaquita Fault brings the Mondaca Strata (~22-21 Ma) atop the mid-Miocene volcanic
424 sequence (El Yunque Volcanic Unit, 15-14 Ma, Mpodozis and Cornejo 2012). This geological
425 evidence together with the new thermochronology data suggest that the cooling/exhumation
426 event during porphyry emplacement (Fig. 6b) was linked to uplift/erosion in the Middle to Late
427 Miocene that was associated with faulting between structural Domains 1 and 2 (Fig. 2). The (U-
428 Th)/He ages of the Eocene del Medio Pluton (15.02 and 12.98 Ma) reflect a cooling event and
429 interpreted uplift of structural Domain 3 in the study region (Figs. 5b-c and 6b).
430
431 **Implications of rapid exhumation and metal endowment**
432 The U-Pb zircon, Re-Os molybdenite and (U-Th)/He ages show that mineralization at
433 Altar formed penecontemporaneously with the emplacement of porphyry stocks that together
434 were rapidly exhumed. Telescoping of porphyry mineralization and the roots of the high
435 sulfidation epithermal system is more evident in the Altar Central deposit, where epithermal
436 enargite-bearing E veins cross-cut the early potassic alteration stage A and B veins (Zwahlen et

al. 2014; Maydagán et al. 2015). Although there are no ages for the sulfides of the epithermal E veins, the superposition of porphyry and epithermal veins, coupled with the U-Pb, Re-Os and (U-Th)/He ages indicate that exhumation continued during the formation of the Central Altar deposit and permitted the telescoping of porphyry and epithermal mineralization, ultimately enhancing the ore grade at Altar. Based on correlation analysis of assay results and mapped abundances of vein types, approximately 11 to 26 % of the copper in the Altar Central orebody is associated with enargite veins, with the bulk of the mineralization being hosted by the early stockwork veining and potassic alteration (Zwahlen et al. 2014). In the Altar Central deposit, this overlap also leads to higher grades in the supergene enrichment zone (Maydagán et al. 2015). In other centers at Altar (e.g. Altar East), this overlap is not so obvious, but veins and disseminations of enargite, bornite, tennantite with gold, locally increase the grades of copper and gold. As such, without the uplift and telescoping, Altar would have been a considerably less economic deposit. This is also likely for many other porphyry systems that have superimposed epithermal mineralization (e.g., Agua Rica porphyry and Famatina mining district in Argentina, Pudack et al. 2009; Franchini et al. 2011, 2015), show hypogene copper enrichment (e.g., Chuquicamata, Ossandón et al. 2001) or are affected by syn-mineral exhumation (e.g., Los Pelambres deposit, Bertens et al. 2006; Perelló et al. 2012).

Regional tectonic implications and relationships to mineralization

A better understanding of the relationships between tectonism (exhumation/uplift) and copper ± molybdenum ± gold mineralization in the Altar-Los Pelambres region requires a broader regional view considering previous regional geochronological and thermochronological studies (Cembrano et al. 2003; Parada et al. 2005, Morata et al. 2010; Ferrando et al. 2014; Lossada et al. 2017, Fig. 7).

The most distinctive geological unit in the central part of the Coastal Range, corresponds to the Early Cretaceous Illapel Plutonic Complex (IPC) dated between 118 ± 1.9 to 96 ± 3 Ma (U-Pb zircon and titanite, and $^{39}Ar/^{40}Ar$ and K/Ar ages, Morata et al. 2006, 2010; Rivano et al. 1993, 1985; Ferrando et al. 2014). Further east, in the eastern Coastal Range Late Cretaceous

465 and Paleocene volcanic sequences are intruded by Paleocene to Eocene granitoids. These
466 include the Late Eocene Fredes-Tres Quebradas pluton (39.1 ± 0.9, 35.5 ± 0.7 Ma) in the north
467 and the Paleocene Manque Bajo (64.7 ±1.8 Ma) and Cuncumén plutons (62-59 Ma) in the south
468 (all U-Pb zircon ages; Mpodozis 2016; Rodríguez et al. 2018, Fig. 7).
469 Following crystallization and cooling, the IPC experienced slow cooling and exhumation,
470 as reflected by the AFT ages (68.3 ± 3.8 and 41.4 ± 4.4 Ma; Rodríguez et al. 2018), which show
471 that the IPC crossed the 110°C isotherm during the Paleocene-Eocene, while (U-Th)/He ages
472 (31.5 ± 1.6 and 23.5 ± 6.5 Ma) indicate that cooling below 70°C occurred much later, in the
473 Late Oligocene (Rodríguez et al. 2018). In contrast, AFT and (U-Th)/He ages from the
474 Paleocene to Eocene plutons of the eastern Coastal Range (Domain 4) record rapid cooling and
475 uplift events after pluton emplacement. The AFT ages between 41.7 ± 5 and 30 ± 3.2 Ma
476 indicate that the Late Eocene Fredes-Tres Quebradas pluton cooled to the apatite partial
477 annealing zone temperature (125 - 60º C) rapidly following emplacement. Further cooling to
478 ≤70˚C by the Middle Miocene is evidenced from the 18.1 ± 1.2 to 10 ± 1.4 Ma (U-Th)/He ages
479 (Rodríguez et al. 2018; Fig. 7). A similar cooling path to 125 – 70˚C and <70˚C since the
480 Eocene is shown by the AFT (43.7 Ma) and (U-Th)/He (10.5 Ma) ages of the, older, Early
481 Paleocene Manque Bajo stock. However, the data set from the southernmost Cuncumén pluton
482 (62 – 59 Ma, Fig. 7) is more difficult to interpret as the AFT (16 Ma) and (U-Th)/He (6.9 Ma)
483 ages (Rodríguez et al. 2018) are younger. This discrepancy is perhaps related to the fact that this
484 intrusive body displays extensive tectonic damage (brecciation, cataclasis) and is located right
485 along the northern termination of the Pocuro Fault, which extends many kilometers to the south
486 along the western slope of the Main Cordillera in the Los Pelambres region (Carter and Aguirre
487 1965; Rivano and Sepúlveda 1991; Mpodozis et al. 2009, Fig. 7).
488 Despite this exception, the available data suggest that at the latitude of Altar-Los
489 Pelambres exhumation and uplift progressed episodically from west to east during the
490 Cretaceous and the Miocene (Rodríguez et al. 2018). The IPC (Fig. 7) probably began to be
491 exhumed as consequence of the onset of Andean compressional deformation in the early Late
492 Cretaceous (Mpodozis and Ramos 1989).

493 Younger events, recorded further east in the great Altar-Los Pelambres region, include an
494 episode of rapid exhumation in the Late Eocene. This event agrees with the results of
495 thermochronological studies in the Elqui valley, in Chile, at 30°S, that indicate a period of rapid
496 cooling between 35 and 30 Ma (Cembrano et al. 2003; Lossada et al. 2007). This event
497 coincides with the beginning of foredeep sedimentation in Argentina, where sediments derived
498 from the western highlands started to accumulate in the Bermejo foreland basin during the Late
499 Eocene (Fosdick et al. 2017). The rapid cooling/exhumation in the Eocene can be related to the
500 deformation associated with the Incaic Tectonic Event (Steinmann 1929) recognized along the
501 whole Central Andes north of 28°S that was accompanied by the formation of the Bolivian
502 Orocline (Arriagada et al. 2008) and the emplacement of the Late Eocene-Early Oligocene
503 intrusions of the southern Peru-northern Chile porphyry copper province (Sillitoe and Perelló
504 2005).
505 The Early Oligocene-Late Oligocene "slow cooling" period observed at 30°S in the Elqui
506 valley region (Lossada et al. 2017) coincides, with the intense volcanic activity that gave rise to
507 the Pelambres and Pachón formations and the Mondaca and Río Chicharra Strata which
508 accumulated at the northern end of the Central Chile Abanico/Coya Machalí extensional intra
509 arc basin (Charrier et al. 2002, 2005; Mpodozis and Cornejo 2012). Volcanism occurred during
510 a period of fast plate convergence rates (Jordan et al. 2001) causing steady westward
511 displacement of the South American Plate (Silver et al. 1998; Kay and Copeland 2006) and
512 weak intraplate coupling (Mpodozis and Cornejo 2012; Horton and Fuentes 2016) when
513 ensuing extensional conditions permitted the production and ascent of large volumes of magmas
514 (Mpodozis and Cornejo 2012; Horton and Fuentes 2016).
515 A second period of rapid cooling in the Elqui Valley (30°S, Lossada et al. 2017) in the
516 Early Miocene (ca. 18 Ma) agrees with the 18-15 Ma (U-Th)/He ages obtained in the Domain 4
517 in the Fredes-Tres Quebradas plutons (Rodriguez et al. 2018, Fig. 7). At this time there is clear
518 evidence of tectonic activity in the Altar-Pelambres region where field relationships indicate
519 that the Pelambres Fault was active as a thrust fault between 18 and 14 Ma (Mpodozis et al.
520 2009; Perelló et al. 2012). This event has been also well recognized in Chile and Argentina

south of 32°S (Giambiagi et al. 2012; Piquer et al. 2017; Buellow et al. 2018) matching with the beginning of deformation and collapse (inversion) of the extensional Abanico-Coya Machalí Basin (Charrier et al. 2002, 2005; Piquer et al. 2017) and initiation of the shallowing of the subducted Nazca slab, as intraplate coupling between the Nazca and South American Plates increased and convergence rates decreased (Kay and Mpodozis 2002; Mpodozis and Cornejo 2012; Horton and Fuentes 2016).

The younger (U-Th)/He ages obtained at Altar (~15-11 Ma), Los Pelambres and Pachón (~10-8.1 Ma) indicate very fast, almost instantaneous cooling (and exhumation) during the emplacement of porphyry copper intrusions in Domain 2. Exhumation was again related (and triggered) by active deformation as shown by the post 14 Ma activity documented for the Mondaquita Fault and further east, by the transport of the basement blocks of Santa Cruz and Espinacito ranges of the Frontal Cordillera over the < 18 Ma synorogenic sedimentary strata of the Manantiales foreland basin (Jordan et al. 1996; Pérez 2001; Alarcón and Pinto 2015). Compressional deformation generated crustal shortening through hybrid thin and thick-skinned thrusting (e.g. Cristallini and Ramos 2000; Giambiagi et al. 2003). Crustal thickening during uplift of the Frontal Cordillera and eastward migration of the magmatic front seems to have created the favorable conditions for the generation of water-rich, high Sr/Y "adakitic" magmas at Altar and Los Pelambres (Perelló et al. 2012; Maydagán et al. 2014; Bergoeing 2016) whose presence has been shown to be critical for the formation of most of the porphyry copper deposits around the world (Kay and Mpodozis 2001; Chiaradia et al. 2012; Richards 2011). Porphyry copper mineralization and deformation at ~11-10 Ma coincides with arrival at the trench and beginning of subduction of the E-trending segment of the Juan Fernández Ridge hotspot track below the Los Pelambres-Altar region (Yañez et al. 2001, 2002). Recent studies indicate that the shallowest portion of the flat-slab is associated with the actual inferred location of the subducting Juan Fernández Ridge directly below the Altar-Los Pelambres at 31-32°S (Anderson et al. 2007; Ammiratti et al. 2016). Some authors have proposed a close link between the subduction of aseismic ridges and porphyry copper mineralization (Rosenmbaum et al. 2005; Sun et al. 2010). In adittion, tectonic perturbations on the downgoing slab could have

549 generated changes in the tectonic stress regime in the crust favorable for magma emplacement
550 and ore formation (Hollings et al. 2005; Maydagán et al. 2011). However, recently, Cu-rich
551 porphyry systems with the same age of 10 - 11 Ma (Valeriano, Los Helados, Sillitoe and Perelló
552 2005; Sillitoe et al. 2016) have been discovered along the Chilean-Pampean flat slab region, up
553 to 400 km north from the Altar-Pelambres, that seem to be located too far north to be directly
554 influenced by the Juan Fernández Ridge subduction. A similar argument can be made for the
555 giant deposits located to the south, where the U-Pb, $^{40}Ar/^{39}Ar$, K-Ar and Re-Os ages of the
556 intrusions related to the copper mineralization, between 6.3 ± 0.1 and 4.3 ± 0.1 Ma at Río
557 Blanco-Los Bronces (Deckart et al. 2014) and between 6.5 ± 0.1 to 4.3 ± 0.1 Ma at El Teniente
558 porphyry deposit (Maksaev et al. 2004; Deckart et al. 2005), seem to be young to be directly
559 linked to the 11-10 Ma subduction of the E-trending Juan Fernández Ridge arm at 31-32°.
560 If the relationship between Juan Fernández Ridge subduction and generation of fertile
561 copper-enriched magmas is not straight forward, the connection of ridge subduction with rapid
562 cooling, uplift and exhumation needs to be analyzed. Recent studies have analyzed this
563 relationship in the Pampean flat-slab segment of the Andes (Davila and Lithgow-Bertelloni
564 2013; Stevens Goddard and Carrapa 2018). Davila and Lithgow-Bertelloni (2015) suggested
565 that the collision and subduction of thick aseismic volcanic ridges, like the Juan Fernández
566 Ridge, may drive dynamic uplift in the Andean margin. Examples in other segments of the
567 south American plate are the collision of the Carnegie Ridge in northern Ecuador and the
568 subduction of the Nazca Ridge in southern Peru, where the ridge acted as a wave uplifting the
569 Andean margin as it moved slowly southwards during the Miocene (Wipft et al. 2008; Spikings
570 and Simpson 2014). Another case possibly occurs in the southern Patagonian Andes, where
571 episodic cooling and exhumation results from the subduction of the active Chile Ridge (Ramos
572 2005; Haschke et al. 2006; Guillaume et al. 2009; Georgieva et al. 2019; Stevens Goddard and
573 Fosdick 2019).
574 AFT data for Miocene plutons of the Main Andean Range in Chile between 33-35°S,
575 south of the location of the subducted E-trending segment of the Juan Fernández Ridge, define a
576 younger and distinct <10 Ma episode of enhanced crustal cooling through the temperature range

577 of the apatite partial annealing zone (~125-60°C) between 6 and 3 Ma (Maksaev et al. 2009)
578 that cannot be the result of Juan Fernández Ridge subduction. Together with the (U-Th)/He ages
579 for Río Blanco-Los Bronces (3.5 and 2.7 Ma) and El Teniente (3.4 to 2.7 Ma), rapid cooling and
580 exhumation during/after the cessation of igneous and hydrothermal activity occurred at these
581 deposits (McIness et al. 2005) at a much younger time than at Altar-Los Pelambres. Similar (U-
582 Th)/He ages between 6 and 2 Ma are shown for the Abanico and Farellones formations between
583 33-34°S (Piquer et al. 2017). Also, AFT and (U-Th)/He ages, and numerical models of
584 knickpoint retreat carried out between 33 and 35°S indicate that >2 km of uplift have occurred
585 since 10.5 - 4.6 Ma as a consequence of tectonic shortening and "out of sequence" thrusting
586 (Farías et al. 2008). At these latitudes, to the east, accelerated cooling, rock uplift and river
587 incision lasting to present day, initiated at ~10 - 9 Ma in the Argentine Frontal Cordillera as a
588 consequence of progressive thrusting of the Frontal Cordillera over the sedimentary fill of the
589 Tunuyán foreland basin (Hilley et al. 2004; Giambiagi et al. 2014; Hoke et al. 2014).
590 The new data presented here indicate a pulse of rapid cooling/exhumation in the Main
591 Andean Range, at 31-32°, between 15 and 10 Ma. This event was not recorded by Lossada et al.
592 (2017) in the High Andes at 30°S (Elqui Valley) who indicated that only minor erosion,
593 exhumation and modification of topography has occurred there since the Early Miocene.
594 Slightly older (U-Th)/He ages (18-16 Ma) and similar (U-Th)/He ages (15-10 Ma) were
595 reported by Rodriguez et al. (2018) west of the study area in Chile (Fig. 7). In the Argentine
596 Precordillera and in the foreland, late Miocene and Pliocene cooling ages have been reported
597 (Fosdick et al. 2015; Ortiz et al. 2015; Stevens Goddard and Carrapa 2018).
598 The Middle-Late Miocene pulse of rapid cooling/exhumation in the study region (15-10
599 Ma) coincides with tectonic shortening associated with the flattening of the subducted Nazca
600 slab. The youngest (U-Th)/He ages (11-10 Ma) also coincide with the collision of the E-
601 trending arm of the Juan Fernández Ridge with the trench at these latitudes (Yañez et al. 2001).
602 The ridge subduction seems to be, at least temporally, connected with the pulse of rapid
603 exhumation during the emplacement of the porphyry copper-epithermal deposits in the Main

Andean Range at 31-32°S. However, more regional (U-Th)/He dating would be necessary to determine the extent and distribution of this rapid cooling/exhumation event.

Conclusions

The new (U-Th)/He data presented for El Altar indicate a pulse of rapid cooling/exhumation in the Main Andean Range of Argentina and Chile, at 31°30' S, between 15 and 11 Ma. The (U-Th)/He and Re-Os data presented here, in combination with previous U-Pb geochronology, demonstrate that the exhumation pulse occurred simultaneously with the intrusion of the subvolcanic stocks associated with the Cu-Au mineralization in the Altar deposit, and slightly prior to the exhumation in Los Pelambres deposit. The rapid uplift and exhumation during the formation of the hydrothermal system affected the metal (Cu-Au grades) endowment, by the telescoping of the porphyry system and epithermal mineralization. Without this process the porphyry deposits would have been less economic, with the porphyry system remaining at considerable depth.

This Middle-Late Miocene pulse of exhumation coincides with tectonic shortening associated with the flattening of the subducted Nazca slab and with the collision of the E-trending arm of the Juan Fernández Ridge with the trench, at 11-10 Ma, at this latitude. The ridge subduction seems to be, at least temporally, connected with the pulse of rapid exhumation during the emplacement of the porphyry copper-epithermal deposits in the studied region.

References

Aguirre L (1960) Geología de los Andes de Chile Central, Provincia de Aconcagua. Inst Invest Geol 9, Santiago de Chile

Alarcón P, Pinto L (2015) Neogene erosion of the Andean Cordillera in the flat-slab segment as indicated by petrography and whole-rock geochemistry from the Manatiales Foreland Basin (32°-32°30´S). Tectonophys 639: 1-22

630 Aldebaran Resources (2018) Resources Report. www.aldebaranresources.com
631 Alvarez PP (1996) Los depósitos triásicos y jurásicos de la Alta cordillera de San Juan:
632 Geología de la región del Aconcagua provincias de San Juan y Mendoza. Dir Nac Serv
633 Geol Buenos Aires 24 (5): 59–137
634 Ammirati JB, Luján SP, Alvarado P, Beck S, Rocher S, Zandt G (2016) High-resolution images
635 above the Pampean flat slab of Argentina (31–32 S) from local receiver functions:
636 Implications on regional tectonics. Earth Planet Sci Lett 450: 29-39
637 Anderson M, Alvarado P, Zandt G, Beck S (2007) Geometry and brittle deformation of the
638 subducting Nazca Plate, Central Chile and Argentina. Geophys J Inter 171(1): 419-434
639 Arriagada C, Roperch P, Mpodozis C, Cobbold PR (2008) Paleogene building of the Bolivian
640 Orocline: Tectonic restoration of the central Andes in 2-D map view. Tectonics
641 https://doi:10.1029/2008TC002269
642 Bergoeing JP (2016) Evolución geoquímica del magmatismo de la Región de Los Pelambres
643 (31°S) entre el Cretácico superior y el Mioceno superior: Implicancias para la evolución
644 tectónica y metalogénica de los Andes de Chile Central. Bch Thesis, Departamento de
645 Geología, Universidad de Chile, Santiago, 131 p
646 Bertens A, Deckart K, Gonzalez A (2003) Geocronología U-Pb, Re-Os y ^{40}Ar-^{39}Ar del pórfido
647 de Cu-Mo Los Pelambres, Chile central. X Congreso Geológico Chileno, 1 p
648 Bertens A, Clark A, Barra F, Deckart K (2006) Evolution of the Los Pelambres-El Pachón
649 porphyry copper-molybdenum district, Chile-Argentina. XI Congreso Geológico Chileno
650 2:179-181
651 Buelow EK, Suriano J, Mahoney JB, Kimbrough DL, Mescua JF, Giambiagi LB, Hoke GD
652 (2018) Sedimentologic and stratigraphic evolution of the Cacheuta basin: Constraints on
653 the development of the Miocene retroarc foreland basin, south-central Andes. Lithosphere
654 10(3): 366-391
655 Cahill T, Isacks BL (1992) Seismicity and shape of the subducted Nazca plate. J of Geophys
656 Res: Solid Earth, 97(B12): 17503-17529

Carter W, Aguirre Le-Bert L (1965) Structural geology of Aconcagua province and its relationship to the central valley graben, Chile. Geol Soc Am Bull 76(6) :651-664

Cembrano J, Zentilli M, Grist A, Yáñez G (2003) Nuevas edades de trazas de fisión para Chile Central (30°-34°S): Implicancias en el alzamiento y exhumación de los Andes desde el Cretácico. X Congreso Geológico Chileno, 5 p

Charrier R, Baeza O, Elgueta S, Flynn J, Gans P, Kay SM, Muñoz N, Wyss, Zurita E (2002) Evidence for Cenozoic extensional Basin development and Tectonic Inversion, south of the flat -slab segment, southern Central Andes, Chile (33°-36°) J S Am Earth Sci 15: 117-139

Charrier R, Bustamante M, Comte D, Elgueta S, Flynn JJ, Iturra N, Muñoz N, Pardo M, Thiele, Wyss AR (2005) The Abanico Extensional Basin: regional extension, chronology of tectonic inversion and relation to shallow seismic activity and Andean uplift. Neues Jahrbuch für Geologie und Paläontologie, Abhandlungen 236: 43-77

Chiaradia M, Ulianov A, Kouzmanov K, Beate B (2012) Why large porphyry Cu deposits like high Sr/Y magmas? Sci Rep 2, 68

Cioldi S (2009) The Altar Exploration Project: Geology and hydrothermal mineralization paragenesis of the Cu-Mo-Au porphyry deposit, San Juan Province, Argentina, Master thesis, ETH Zurich, 68 p

Collo G, Dávila FM, Nóbile J, Astini RA, Gehrels G (2011) Clay mineralogy and thermal history of the Neogene Vinchina Basin, central Andes of Argentina: Analysis of factors controlling the heating conditions. Tectonics 30 (4)

Cooke DR, Hollings P, Walshe JL (2005) Giant porphyry deposits: characteristics, distribution, and tectonic controls. Econ Geol 100(5): 801-818

Cristallini EO, Ramos VA (2000) Thick-skinned and thin-skinned thrusting in the La Ramada fold and thrust belt: crustal evolution of the High Andes of San Juan, Argentina (32 SL). Tectonophys 317(3): 205-235

Dávila FM, Lithgow-Bertelloni C (2013). Dynamic topography in South America. J S Am Earth Sci 43: 127-144

685 Dávila FM, Lithgow-Bertelloni C (2015) Dynamic uplift during slab flattening. Earth Planet Sci
686 Lett 425: 34-43
687 Deckart K, Clark AH, Aguilar C, Vargas R, Bertens A, Mortensen JK, Fanning M (2005)
688 Magmatic and hydrothermal geochronology of the giant Río Blanco porphyry copper
689 deposit, central Chile: Implications of an integrated U-Pb and $^{40}Ar/^{39}Ar$ database. Econ
690 Geol 100: 905-934
691 Deckart K, Silva W, Spröhnle C, Vela I (2014) Timing and duration of hydrothermal activity at
692 the Los Bronces porphyry cluster: An update. Miner Deposita 49(5): 535-546
693 Farías M, Charrier R, Carretier S, Martinod J, Fock A, Campbell D, Comte D (2008) Late
694 Miocene high and rapid surface uplift and its erosional response in the Andes of central
695 Chile (33–35 S). Tectonics 27(1)
696 Farley KA (2002) (U-Th)/He dating: techniques, calibrations, and applications. Rev Min
697 Geochem 47: 819-844
698 Fernández RR, Brown RF, Lencinas AN (1974) Pachón, un nuevo pórfiro cuprífero argentino,
699 Departamento de Calingasta, provincia de San Juan, República Argentina. V Congreso
700 Geológico Argentino 2: 77-89
701 Ferrando R, Roperch P, Morata D, Arriagada C, Ruffet G Córdova ML (2014) A paleomagnetic
702 and magnetic fabric study of the Illapel Plutonic Complex, Coastal Range, central Chile:
703 Implications for emplacement mechanism and regional tectonic evolution during the mid-
704 Cretaceous. J S Am Earth Sci 50: 12-26
705 Fillon C, Gautheron C, van der Beek P (2013) Oligocene–Miocene burial and exhumation of the
706 Southern Pyrenean foreland quantified by low-temperature thermochronology. J Geol Soc
707 170(1): 67-77
708 Fitzgerald PG, Baldwin SL, Webb LE, O'Sullivan PB (2006) Interpretation of (U–Th)/He single
709 grain ages from slowly cooled crustal terranes: a case study from the Transantarctic
710 Mountains of southern Victoria Land. Chem Geol 225(1-2): 91-120

711 Fosdick JC, Carrapa B, Ortíz G (2015) Faulting and erosion in the Argentine Precordillera
712 during changes in subduction regime: Reconciling bedrock cooling and detrital records.
713 Earth Planet Sci Lett 432: 73-83
714 Fosdick JC, Reat EJ, Carrapa B, Ortiz G, Alvarado PM (2017) Retroarc basin reorganization
715 and aridification during Paleogene uplift of the southern central Andes. Tectonics 36(3):
716 493-514
717 Fournier RO (1999) Hydrothermal processes related to movement of fluid from plastic into
718 brittle rock in the magmatic-epithermal environment. Econ Geol 94(8): 1193-1211
719 Franchini M, Impiccini A, Lentz D, Ríos J, O'Leary S, Pons J, Schalamuk A (2011) Porphyry to
720 epithermal transition in the Agua Rica polymetallic deposit, Catamarca, Argentina: An
721 integrated petrologic analysis of ore and alteration parageneses. Ore Geol Rev 41:49-74
722 Franchini M, McFarlane C, Maydagán L, Reich M, Lentz D, Meinert L, Bouhier V (2015)
723 Trace metals in pyrite and marcasite from the Agua Rica porphyry-high sulfidation
724 epithermal deposit, Catamarca, Argentina: Textural features and metal zoning at the
725 porphyry to epithermal transition. Ore Geol Rev 66: 366-387
726 Gautheron C, Tassan-Got L (2010) A Monte Carlo approach to diffusion applied to noble
727 gas/helium thermochronology. Chem Geol 273(3): 212-224
728 Gautheron C, Tassan-Got L, Ketchamand RA, Dobson KJ (2012) Accounting for long alpha-
729 particle stopping distances in (U–Th–Sm)/He geochronology: 3D modeling of diffusion,
730 zoning, implantation, and abrasion, Geochim Cosmochim Acta 96: 44-56
731 Georgieva V, Gallagher K, Sobczyk A, Sobel ER, Schildgen TF, Ehlers TA, Strecker MR
732 (2019) Effects of slab-window, alkaline volcanism, and glaciation on thermochronometer
733 cooling histories, Patagonian Andes. Earth Pl Sci Lett 511: 164-176
734 Giambiagi L, Ramos V, Godoy E, Alvarez PP, Orts S (2003) Cenozoic deformation and
735 tectonic style of the Andes, between 33° and 34° south latitude. Tectonics 22(4)
736 Giambiagi L, Mescua J, Bechis F, Tassara A, Hoke G (2012) Thrust belts of the Southern
737 Central Andes: along strike variations in shortening, topography, crustal geometry and
738 denudation. Geol Soc Am Bull 124(7-8): 1339-1351

739 Giambiagi L, Tassara A, Mescua J, Tunik M, Alvarez PP, Godoy E, Hoke G, Pinto L,
740 Spagnotto S, Poirras H, Tapia F, Jara P, Bechis F, García V, Suriano J, Moreiras SM,
741 Pagano S (2014) Evolution of shallow and deep structures along the Maipo–Tunuyán
742 transect (33 40' S): from the Pacific coast to the Andean foreland. Geol Soc London Spec
743 Pub 399, http://dx.doi.org/10.1144/SP399.14
744 Guillaume B, Martinod J, Husson L, Roddaz M, Riquelme R (2009) Neogene uplift of central
745 eastern Patagonia: Dynamic response to active spreading ridge subduction?. Tectonics
746 28(2)
747 Haddon, A., Porter. R, (2018) S- Wave Receiver Function Analysis of the Pampean Flat- Slab
748 Region: Evidence for a Torn Slab. Geochem Geophys Geosys 19(10): 4021-4034
749 Haschke M, Sobel ER, Blisniuk P, Strecker MR, Warkus F (2006) Continental response to
750 active ridge subduction. Geophys Res Lett 33(15)
751 Hilley GE, Strecker MR, Ramos VA (2004) Growth and erosion of fold-and-thrust belts with an
752 application to the Aconcagua fold-and-thrust belt, Argentina. J Geophys Res Solid Earth
753 109 (B1).
754 Hoke GD, Graber NR, Mescua JF, Giambiagi LB, Fitzgerald PG, Metcalf JR (2014) Near pure
755 surface uplift of the Argentine Frontal Cordillera: insights from (U–Th)/He
756 thermochronometry and geomorphic analysis. Geol Soc London Spec Pub 399
757 http://dx.doi.org/10.1144/SP399.4
758 Hollings P, Cooke D, Clark A (2005) Regional geochemistry of Tertiary igneous rocks in
759 central Chile: Implications for the geodynamic environment of giant porphyry copper and
760 epithermal gold mineralization. Econ Geol 100(5): 887-904
761 Horton BK, Fuentes F (2016) Sedimentary record of plate coupling and decoupling during
762 growth of the Andes. Geol 44(8): 647-650
763 House MA, Wernicke BP, Farley KA (1998) Dating topography of the Sierra Nevada,
764 California, using apatite (U–Th)/He ages. Nature 396 (6706), 66

765 Irarrazaval V, Sillitoe RH, Wilson A, Toro JC, Robles W, Lyall G (2010) Discovery history of a
766 giant, high-grade, hypogene porphyry copper molybdenum deposit at Los Sulfatos, Los
767 Bronces-Rio Blanco district, central Chile: Soc Econ Geol Spec Pub 15: 253–269
768 Jordan TE, Tamm V, Figueroa G, Flemings PB, Richards D, Tabbutt K, Cheatham T (1996)
769 Development of the Miocene Manantiales foreland basin, Principal Cordillera, San Juan,
770 Argentina. Andean Geol 23(1): 43-79
771 Jordan TE, Burns WM, Veiga R, Pángaro F, Copeland P, Kelley S, Mpodozis C (2001)
772 Extension and basin formation in the southern Andes caused by increased convergence
773 rate: A mid-Cenozoic trigger for the Andes. Tectonics 20(3): 308-324
774 Kay SM, Mpodozis C (2001) Central Andean ore deposits linked to evolving shallow
775 subduction systems and thickening crust. GSA Today 11: 4–9
776 Kay SM, Mpodozis C (2002) Magmatism as a probe to the Neogene shallowing of the Nazca
777 plate beneath the modern Chilean flat-slab. J S Am Earth Sci 15: 39-57
778 Kay SM, Copeland P (2006) Early to middle Miocene back-arc magmas of the Neuquén basin
779 of the southern Andes: Geochemical consequences of slab shallowing and the westward
780 drift of South America (35°–39° S lat.): Geol Soc Am Spec Paper 40: 185–213
781 Klohn C (1960) Geología de la Cordillera de los Andes de Chile Central, provincias de
782 Santiago, O'Higgins, Colchagua y Curicó. Inst Invest Geol (Chile) 8, 95 p
783 Kraml M, Pik R, Rahn M, Selbekk R, Carignan J, Keller J (2006) A new multi-mineral age
784 reference material for $^{40}Ar/^{39}Ar$, (U-Th)/He and fission track dating methods: the Limberg
785 t3 tuff. Geostand and Geoanalytical Res 30(2): 73-86
786 Lencinas A, Tonel M (1993) La Brecha Sur del Yacimiento de Cobre Porfídico de Pachón, San
787 Juan, República Argentina. XI Congreso Geológico Argentino pp 241-247
788 Li Y, Selby D, Feely M, Costanzo A, Li XH (2017) Fluid inclusion characteristics and
789 molybdenite Re-Os geochronology of the Qulong porphyry copper-molybdenum deposit,
790 Tibet. Miner Deposita 52(2): 137-158

791 Lossada AC, Giambiagi L, Hoke GD, Fitzgerald PG, Creixell C, Murillo I, Suriano J (2017)
792 Thermochronologic evidence for late Eocene Andean mountain building at 30°
793 S. Tectonics 36(11): 2693-2713
794 Luijendijk E (2019) Beo v1.0: Numerical model of heat flow and low-temperature
795 thermochronology in hydrothermal systems. Geosci Model Dev
796 https://doi.org/10.5194/gmd-2018-341.
797 Mackaman-Lofland C, Horton BK, Fuentes F, Constenius KN, Stockli DF (2019) Mesozoic to
798 Cenozoic retroarc basin evolution during changes in tectonic regime, southern Central
799 Andes (31–33°S): Insights from zircon U-Pb geochronology. J S Am Earth Sci 89: 299-
800 318
801 Maksaev V, Munizaga F, McWilliams M, Fanning M, Mathur R, Ruiz J, Zentilli M (2004) New
802 chronology for El Teniente, Chilean Andes, from U/Pb, $^{40}Ar/^{39}Ar$, Re-Os and fission
803 track dating: Implications for the evolution of a supergiant porphyry Cu-Mo deposit. Soc
804 Econ Geol Spec Pub 11: 15-54
805 Maksaev V, Munizaga F, Zentilli M, Charrier R (2009) Fission track thermochronology of
806 Neogene plutons in the Principal Andean Cordillera of central Chile (33-35 S):
807 Implications for tectonic evolution and porphyry Cu-Mo mineralization. Andean Geol
808 36(2): 153-171
809 Maydagán L (2012) El Prospecto de Cu-(Au-Mo) Altar (31º 29'LS, 70º28'LO), San Juan:
810 Unpublished Ph.D thesis, Bahía Blanca, Argentina, Universidad Nacional del Sur, 340 p
811 Maydagán L, Franchini M, Chiaradia M, Pons J, Impiccini A, Toohey J, Rey R (2011)
812 Petrology of the Miocene igneous rocks in the Altar region, main Cordillera of San Juan,
813 Argentina. A geodynamic model within the context of the Andean flat-slab segment and
814 metallogenesis. J S Am Earth Sci 32(1): 30-48
815 Maydagán L, Franchini M, Chiaradia M, Dilles J, Rey R (2014) The Altar porphyry Cu-(Au-
816 Mo) deposit (Argentina): a complex magmatic-hydrothermal system with evidence of
817 recharge processes. Econ Geol 109(3): 621-641

Maydagán L, Franchini M, Rusk B, Lentz DR, McFarlane C, Impiccini A, Ríos J, Rey R (2015) Porphyry to epithermal transition in the Altar Cu-(Au-Mo) deposit, Argentina, studied by cathodoluminescence, LA-ICP-MS, and fluid inclusion analysis. Econ Geol 110(4): 889-923

Maydagán L, Franchini M, Chiaradia M, Bouhier V, Di Giuseppe N, Rey R, Dimieri, L (2017) Petrogenesis of Quebrada de la Mina and Altar North porphyries (Cordillera of San Juan, Argentina): Crustal assimilation and metallogenic implications. Geosci Front 8(5): 1135-1159

McDowell FW, McIntosh WC, Farley KA (2005) A precise ^{40}Ar–^{39}Ar reference age for the Durango apatite (U–Th)/He and fission-track dating standard. Chem Geol 214(3-4): 249-263

McInnes BIA, Evans NJ, Fu FQ, Garwin S, Belousova E, Griffin WL, Bertens A, Sukarna D, Permanadewi S, Andrew R, Deckart K (2005) Thermal history analysis of selected Chilean, Indonesian and Iranian porphyry Cu-Mo-Au deposits. In: Porter TM (ed) Super Porphyry Copper and Gold Deposits: A Global Perspective. Porter Geoconsultancy Publishing, Adelaide, Australia, pp 27-42

Morata D, Féraud G, Schärer U, Aguirre, L, Belmar M, Cosca M (2006) A new geochronological framework for Lower Cretaceous magmatism in the Coastal Range of central Chile. XI Congreso Geológico Chileno, 2 p

Morata D, Varas MJ, Higgins M, Valencia V, Verhoort J (2010) Episodic emplacement of the Illapel Plutonic Complex (Coastal Cordillera, central Chile): Sr and Nd isotopic, and zircon U–Pb geochronological constraints. South American Symposium on Isotope Geology 7, pp 1300169-7

Mpodozis C (2016) Mapa Geológico Regional del Área de Los Pelambres (escala 1:75.0000). Informe Interno, Antofagasta Minerals, Santiago, Chile

Mpodozis C, Ramos VA (1989) The Andes of Chile and Argentina. In: Ericksen GE, Cañas M T, Reinemund JA (eds.) Geology of the Andes and its Relation to Hydrocarbon and

845 Mineral Resources. Circum-Pacific Council for Energy and Mineral Resources, Earth Sci
846 Series 11, 59–90
847 Mpodozis C, Kay SM (1992) Late Paleozoic to Triassic evolution of the Gondwana margin:
848 Evidence from Chilean Frontal Cordilleran batholiths (28° S to 31°S). Geol Soc Am Bull.
849 104(8): 999-1014
850 Mpodozis C, Rivano S, Parada MA, Vicente JC (1976) Acerca del plutonismo tardi-hercínico
851 en la Cordillera Frontal entre los 30° y 33° sur (Provincia de Mendoza y San Juan,
852 Argentina. V Congreso Geológico Argentino, Bahía Blanca, pp 143-71
853 Mpodozis C, Brockway H, Marquardt C, Perelló J (2009) Geocronología U/Pb y tectónica de la
854 región de Los Pelambres-Cerro Mercedario: Implicancias para la evolución cenozoica de
855 los Andes del centro de Chile y Argentina. XII Congreso Geológico Chileno. S9-059, 4 p
856 Mpodozis C, Cornejo P (2012) Cenozoic tectonics and porphyry copper systems of the Chilean
857 Andes. Soc Econ Geol Spec Pub 16: 329-360
858 Musso RJE, Pérez DJ, Rey R, Toohey J (2012) Geología de las nacientes del río La Pantanosa,
859 Cordillera Frontal (31°33'S), Provincia de San Juan, Argentina, Congreso Geológico
860 Chileno, Santiago, pp 250-251
861 Mutschler FE, Ludington S, Bookstrom AA (2010) Giant porphyry related metal camps of the
862 world—a database: USGS Open-File Report 99-556, Online Version 1.0,
863 http://pubs.usgs.gov/of/1999/of99-556/.
864 Ortiz G, Alvarado P, Fosdick JC, Perucca L, Saez M, Venerdini A (2015) Active deformation in
865 the northern Sierra de Valle Fértil, Sierras Pampeanas, Argentina. J S Am Earth Sci 64:
866 339-350
867 Ossandón CG, Fréraut CR, Gustafson LB, Lindsay DD, Zentilli M (2001) Geology of the
868 Chuquicamata mine: A progress report. Econ Geol 96(2): 249-270
869 Parada MA, Féraud G, Fuentes F, Aguirre L, Morata D, Larrondo P (2005) Ages and cooling
870 history of the Early Cretaceous Caleu pluton: testimony of a switch from a rifted to a
871 compressional continental margin in central Chile. J Geol Soc 162(2): 273-287

872 Perelló J, Sillitoe RH, Mpodozis C, Brockway H, Posso H (2012) Geologic setting and
873 evolution of the porphyry copper-molybdenum and copper-gold deposits at Los
874 Pelambres, central Chile. Soc Econ Geol Spec Pub 16: 79-104
875 Pérez DJ (2001) Tectonic and unroofing history of Neogene Manantiales foreland basin
876 deposits, Cordillera Frontal (32°30'S), San Juan Province, Argentina. J S Am Earth Sci
877 14: 693-705
878 Piquer J, Hollings P, Rivera O, Cooke DR, Baker M, Testa F (2017) Along-strike segmentation
879 of the Abanico Basin, central Chile: New chronological, geochemical and structural
880 constraints. Lithos 268: 174-197
881 Pudack C, Halter WE, Heinrich CA, Pettke T (2009) Evolution of magmatic vapor to gold-rich
882 epithermal liquid: The porphyry to epithermal transition at Nevados de Famatina,
883 northwest Argentina. Econ Geol 104(4): 449-477
884 Ramos VA (2005) Seismic ridge subduction and topography: Foreland deformation in the
885 Patagonian Andes. Tectonophys 399(1-4): 73-86
886 Ramos VA, Jordan TE, Allmendinger RW, Mpodozis C, Kay SM, Cortés JM, Palma M (1986)
887 Paleozoic terranes of the central Argentine-Chilean Andes. Tectonics 5(6): 855-880
888 Regard V, Lagnous R, Espurt N, Darrozes J, Baby P, Roddaz M, Hermoza W (2009)
889 Geomorphic evidence for recent uplift of the Fitzcarrald Arch (Peru): A response to the
890 Nazca Ridge subduction. Geomorphol 107(3-4): 107-117
891 Richards JP (2011) High Sr/Y arc magmas and porphyry Cu-Mo-Au deposits: just add water.
892 Econ Geol 106: 1075–1081
893 Rivano S, Sepúlveda P, Hervé F, Godoy E (1985) Geocronología K-Ar de las rocas intrusivas
894 entre los 31-32 °S, Chile. Rev Geol Chile 24: 63-64
895 Rivano S, Sepúlveda P (1991) Hoja Illapel (1:250.000) Región de Coquimbo. Servicio Nacional
896 de Geología y Minería, Carta Geol Chile 69: 1–132
897 Rivano S, Sepúlveda P, Boric R, Espiñeira P (1993) Mapa Geológico de la Hoja Quillota-
898 Portillo (escala 1: 250.000), V Región de Valparaíso. Carta Geol Chile 73.

899 Rodríguez MP, Charrier R, Brichau S, Carretier S, Farías M, de Parseval P, Ketcham RA (2018)
900 Latitudinal and Longitudinal Patterns of Exhumation in the Andes of North-Central Chile.
901 Tectonics 37(9): 2863-2886
902 Rosenbaum G, Giles D, Saxon M, Betts PG, Weinberg R, Duboz C (2005) Subduction of the
903 Nazca Ridge and the Inca Plateau: Insights into the formation of ore deposits in Peru.
904 Earth Planet Sci Lett 239:18-32
905 Sanchez C, Brichau S, Riquelme R, Carretier S, Bissig T, Lopez C, Mpodozis C, Campos E,
906 Regard V, Hérail G, Marquardt C (2018) Exhumation history and timing of supergene
907 copper mineralisation in an arid climate: New thermochronological data from the
908 Centinela District, Atacama, Chile. Terra Nova 30(1): 78-85
909 Sato AM, Llambías EJ, Basei MA, Castro CE (2015) Three stages in the Late Paleozoic to
910 Triassic magmatism of southwestern Gondwana, and the relationships with the
911 volcanogenic events in coeval basins. J S Am Earth Sci 63: 48-69
912 Seedorff E, Dilles JH, Proffett JM, Einaudi MT, Zurcher L, Stavast WJA., Johnson D, Barton,
913 MD (2005) Porphyry deposits: Characteristics and origin of hypogene features. Econ Geol
914 100: 251-298
915 Selby D, Creaser RA (2004) Macroscale NTIMS and microscale LA-MC-ICP-MS Re-Os
916 isotopic analysis of molybdenite: Testing spatial restrictions for reliable Re-Os age
917 determinations, and implications for the decoupling of Re and Os within molybdenite.
918 Geochim Cosmochim Acta 68(19): 3897-3908
919 Sernageomin (2003) Mapa Geológico de Chile: versión digital. Servicio Nacional de Geología y
920 Minería, Publicación Geológica Digital, No. 4 CD-Room
921 Sillitoe RH (1994) Erosion and collapse of volcanoes: Causes of telescoping in intrusion-
922 centered ore deposits. Geology 22(10): 945-948
923 Sillitoe RH (1995) Exploration and discovery of base-and precious-metal deposits in the circum-
924 Pacific region during the last 25 years. Res Geol 19
925 Sillitoe RH (2010) Porphyry copper systems. Econ Geol 105(1): 3-41

926 Sillitoe RH, Perelló J (2005) Andean copper province: Tectonomagmatic settings, deposit types,
927 metallogeny, exploration, and discovery: Econ Geol 100: 845−890
928 Sillitoe RH, Burgoa C, Hopper D (2016) Porphyry copper discovery beneath the Valeriano
929 lithocap, Chile. SEG Newsl 106: 15-20
930 Sillitoe RH, Devine FA, Sanguinetti MI, Friedman RM (2019) Geology of the Josemaría
931 Porphyry Copper-Gold Deposit, Argentina: Formation, Exhumation, and Burial in Two
932 Million Years. Econ Geol 114(3): 407-426
933 Silver PG, Russo RM, Lithgow-Bertelloni C (1998) Coupling of South American and African
934 plate motion and plate deformation. Science 279(5347): 60-63
935 Spikings R, Simpson G (2014) Rock uplift and exhumation of continental margins by the
936 collision, accretion, and subduction of buoyant and topographically prominent oceanic
937 crust. Tectonics 33(5): 635-655
938 Steinmann G (1929) Geologie yon Peru. C. Winter, Heidelberg, vol. 460
939 Stevens Goddard AL, Carrapa B (2018) Using basin thermal history to evaluate the role of
940 Miocene–Pliocene flat-slab subduction in the southern Central Andes (27 S–30 S). Basin
941 Res 30(3): 564-585
942 Stevens Goddard AL, Fosdick JC (2019) Multichronometer thermochronologic modelling of
943 migrating spreading ridge subduction in southern Patagonia. Geology 47: 555-558
944 Sun W, Ling M, Yang X, Fan W, Ding X, Liang H (2010) Ridge subduction and porphyry
945 copper-gold mineralization: An overview. Science China, Earth Sciences 53(4): 475-484
946 Thiele R (1980) Hoja Santiago, Región Metropolitana. Servicio Nacional de Geología y
947 Minería. Carta Geol Chile, Chile (29) 21
948 Willett SD, Brandon MT (2013) Some analytical methods for converting thermochronometric
949 age to erosion rate. Geochem Geophys Geosys 14(1): 209-222
950 Williams-Jones AE, Heinrich CA (2005) 100th Anniversary special paper: vapor transport of
951 metals and the formation of magmatic-hydrothermal ore deposits. Econ Geol 100(7):
952 1287-1312

953 Wipf M, Zeilinger G, Seward D, Schlunegger F (2008) Focused subaerial erosion during ridge
954 subduction: impact on the geomorphology in south-central Peru. Terra Nova 20: 1–10
955 Wolf RA, Farley KA, Kass DM (1998) Modeling of the temperature sensitivity of the apatite
956 (U–Th)/He thermochronometer. Chem Geol 148(1-2): 105-114
957 Yáñez G, Ranero CR, von Huene R, Díaz J (2001) Magnetic anomaly interpretation across the
958 southern central Andes (32°-34°S): the role of the Juan Fernández Ridge in the late
959 Tertiary evolution of the margin. J Geophys Res 106: 6325-6345
960 Yáñez G, Cembrano J, Pardo M, Ranero C, Selles D (2002) The Challenger–Juan Fernández–
961 Maipo major tectonic transition of the Nazca–Andean subduction system at 33–34 S:
962 geodynamic evidence and implications. J S Am Earth Sci 15(1): 23-38
963 Zeitler PK, Herczeg AL, McDougall I, Honda M (1987) U-Th-He dating of apatite: A potential
964 thermochronometer. Geochim Cosmochim Acta 51(10): 2865-2868
965 Zurcher L (2008) U-Pb Geochronology of Rocks from the Los Azules Porphyry Deposit, San
966 Juan, Argentina. Minera Andes, Inc. progress report, Tucson, Arizona, 8 p
967 Zwahlen C, Cioldi S, Wagner T, Rey R, Heinrich C (2014) The porphyry Cu-(Mo-Au) deposit at
968 Altar (Argentina): Tracing gold distribution by vein mapping and LA-ICP-MS mineral
969 analysis. Econ Geol 109(5): 1341-1358
970

971 **Acknowledgments**

972 This work is part of a project funded by Agencia Nacional de Promoción Científica y
973 Tecnológica (ANPCYT): PICT-2016-2689, CONICET (PIP 330), National University of
974 Comahue (PIN 4-I-209) and University of Padova. We express our appreciation to Kevin
975 Heather, John Black, Javier Robeto, Stanford Foy, Mariano Poodts (Aldebaran Resources) for
976 support to our research studies and to María Isabel Romero, Tadeo Castaño and all staff of
977 Peregrine Argentina S.A.U. for provision of site access, logistic support and help during the
978 field work and sampling. David Selby, thanks Antonia Hoffman, Geoff Nowell, and Chris
979 Ottley for analytical support, and acknowledges the Total Endowment Fund and CUG Wuhan
980 Dida Fund. Finally, we appreciate the support given by the editor-in-chief Georges Beaudoin,

981 the associated editor Peter Hollings, José Piquer and anonymous reviewer for their very helpful
982 comments and reviews.

983

984 **Figure Captions**

985 **Fig. 1 a** Location of the study area (rectangle) in the Pampean Flat-Slab segment relative to
986 depth contours on the Wadati-Benioff zone (Cahill and Isacks 1992; Anderson et al. 2007).
987 Note the actual position of the Juan Fernández Ridge (Yañez et al. 2001), the Central Volcanic
988 Zone and the Southern Volcanic Zone. Metallogenic belts (dark grey), porphyry type deposits
989 (circles), high sulfidation epithermal deposits (triangles) are shown. Abbreviations: EP: El
990 Pachón deposit, EY: El Yunque deposit, JF: Juan Fernández, LP: Los Pelambres deposit. **b**
991 Morphostructural units of the Andes between 31°S and 34°S: Coastal Cordillera, Main
992 Cordillera (Cordillera Principal), Frontal Cordillera, La Ramada and Aconcagua fold and thrust
993 belts, Precordillera and Sierra de Pie de Palo. Location of figures 2, 3 and 7 are shown

994 **Fig. 2** Geological map of the study region between 31°S and 32°S based on Mpodozis (2016).
995 Location of structural domains described in the text, main faults and mineral deposits

996 **Fig. 3** Geologic map of the Altar District showing the location of U-Pb ages from Maydagán et
997 al. (2011, 2012, 2014, 2017) and Mpodozis (2016) and the new U-Th/He ages (this study)

998 **Fig. 4** Samples of B-type veins from Altar East and Altar Central analyzed by Re-Os in
999 molybdenite

1000 **Fig. 5 a** Summary of U-Pb ages from the Altar subvolcanic stocks from Maydagán et al. (2011,
1001 2014, 2017) and the new Re-Os ages from Altar East and Altar Central. **b** Summary of U-Th/He
1002 ages from the study area. **c** Simplified west-east cross section of the Altar District with location
1003 of the thermochronology samples relative to the main faults (Pantanosa Fault and Pachón Fault)

1004 **Fig. 6 a** U-Pb in zircon ages (Maydagán et al. 2011, 2014, 2017) and Re-Os in molybdenite
1005 ages from Altar District, comparison with data from Los Pelambres-Frontera and El Pachón
1006 deposits (Bertens et al. 2006; Perelló et al. 2012). **b** U-Th/He data from the Altar District,

1007 comparison with U-Th/He data from Los Pelambres-Frontera (Perelló et al. 2012) and El
1008 Pachón deposits (Bertens et al. 2006)

1009 **Fig. 7** Geological map of the Coastal Cordillera, Main Cordillera and Frontal Cordillera of
1010 Chile and Argentina between 31°S and 32°S based on Sernageomin (2003) and Mpodozis
1011 (2016). Apatite (U-Th)/He ages are shown together with previous U-Th/He ages and apatite
1012 fission track (AFT) ages (Bertens et al. 2006; Rodríguez et al. 2018). U-Pb ages from the Altar
1013 region are from Maydagán (2012) and Maydagán et al. (2014). U-Pb ages from Los Pelambres
1014 deposit are from Perelló et al. (2012). U-Pb ages from Los Azules, Yunque and Rincones de
1015 Araya deposits are from Zurcher (2008) and Mpodozis and Cornejo (2012)

1016 **Table 1** Summary of the Re-Os data for the analyzed molybdenite samples

1017 **Table 2** Weighted mean U-Th/He ages

Table 1. Summary of the Re-Os data for the analyzed molybdenite samples

Sample	wt (g)	Re (ppm)	±	^{187}Re (ppm)	±	^{187}Os (ppb)	±	Age (Ma)	±#
ALD-178-153	0.020	3546.2	13.2	2228.9	8.3	414.4	1.32	11.16	0.06
A68-440	0.021	1867.6	6.9	1173.8	4.3	203.0	0.64	10.38	0.05

#uncertainty including all sources of analytical uncertainty plus decay constant

Table 2

Table 2. Weighted mean U-Th/He ages

Sample	Lithology	Corr age (Ma)	1s ± age (Ma)	Weighted mean age	Error
		11.53	0.23		
A-1	Subvolcanic stock	12.99	0.27	12.18	0.15
		12.28	0.27		
		30.92	0.97		
A-2	Subvolcanic stock	56.83	2.03	n.c	n.c
		26.17	1.00		
		9.96	0.42		
A-5	Subvolcanic stock	14.87	0.42	12.32	0.26
		12.00	0.53		
		12.72	0.26		
A-24	Pico de Los Sapos Batholith	10.66	0.24	11.87	0.15
		12.68	0.31		
A-16	Subvolcanic stock	0.82	0.04	0.82	0.04
A-22	Subvolcanic stock	11.17	0.40	11.17	0.40
A-17	Subvolcanic stock	14.87	0.49	13.45	0.27
		12.80	0.33		
		15.69	0.53		
A-8	Pico de Los Sapos Batholith	14.90	0.52	14.3	0.29
		12.71	0.47		
		29.63	1.78		
A-12	Chinchimoye Sequence	27.58	1.66	n.c	n.c
		6.15	0.37		
		48.67	2.92		
A-19	Chinchimoye Sequence	55.57	3.33	n.c	n.c
		24.44	1.47		
PDM18	Plutón del Medio	15.02	0.36	13.46	0.17
		12.98	0.20		

Abbreviations: n.c: not calculated.

Figure 1

Click here to access/download;Figure;Fig. 1.jpg

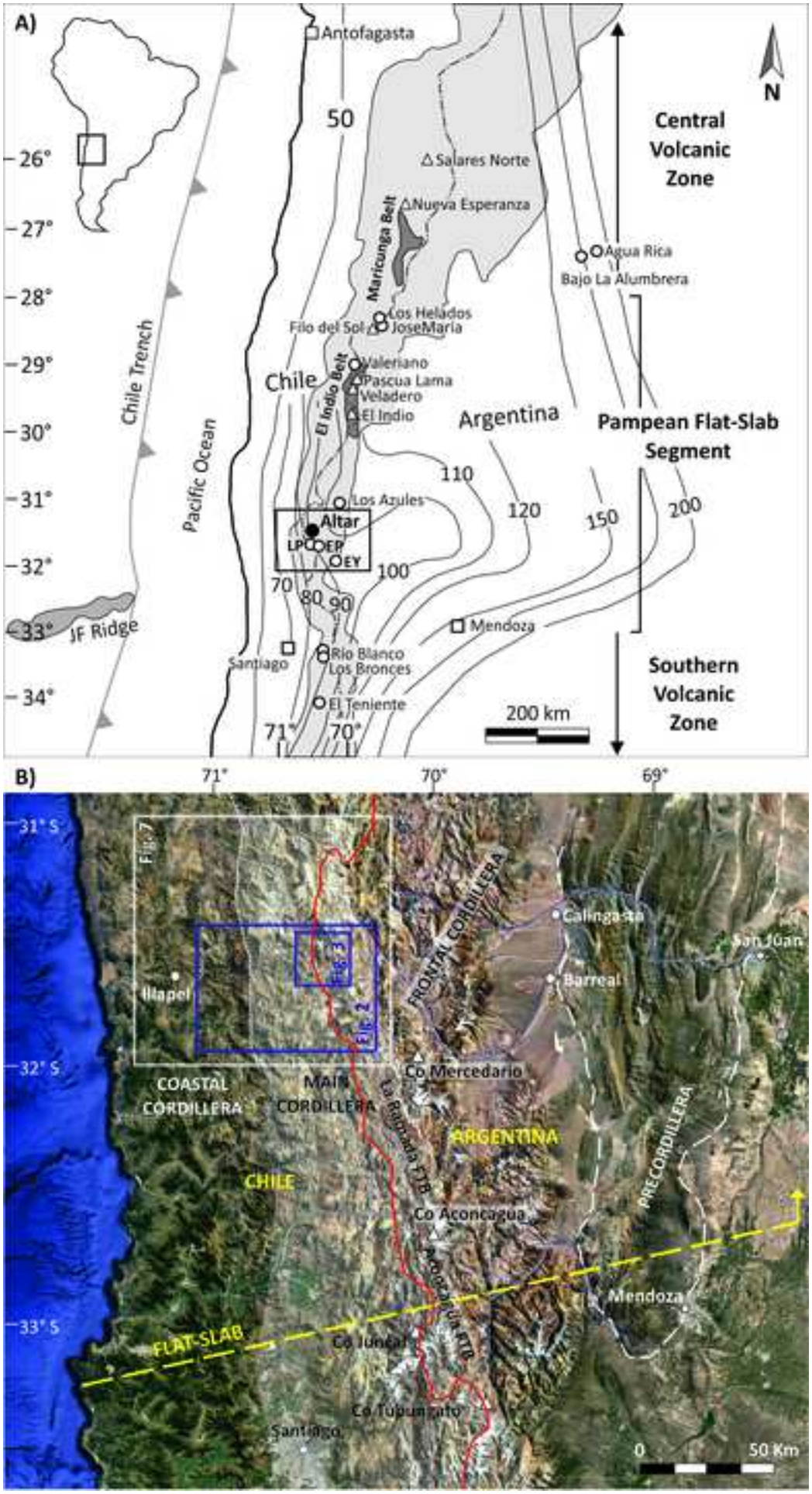

Figure 2

Click here to access/download;Figure;Fig. 2.tif

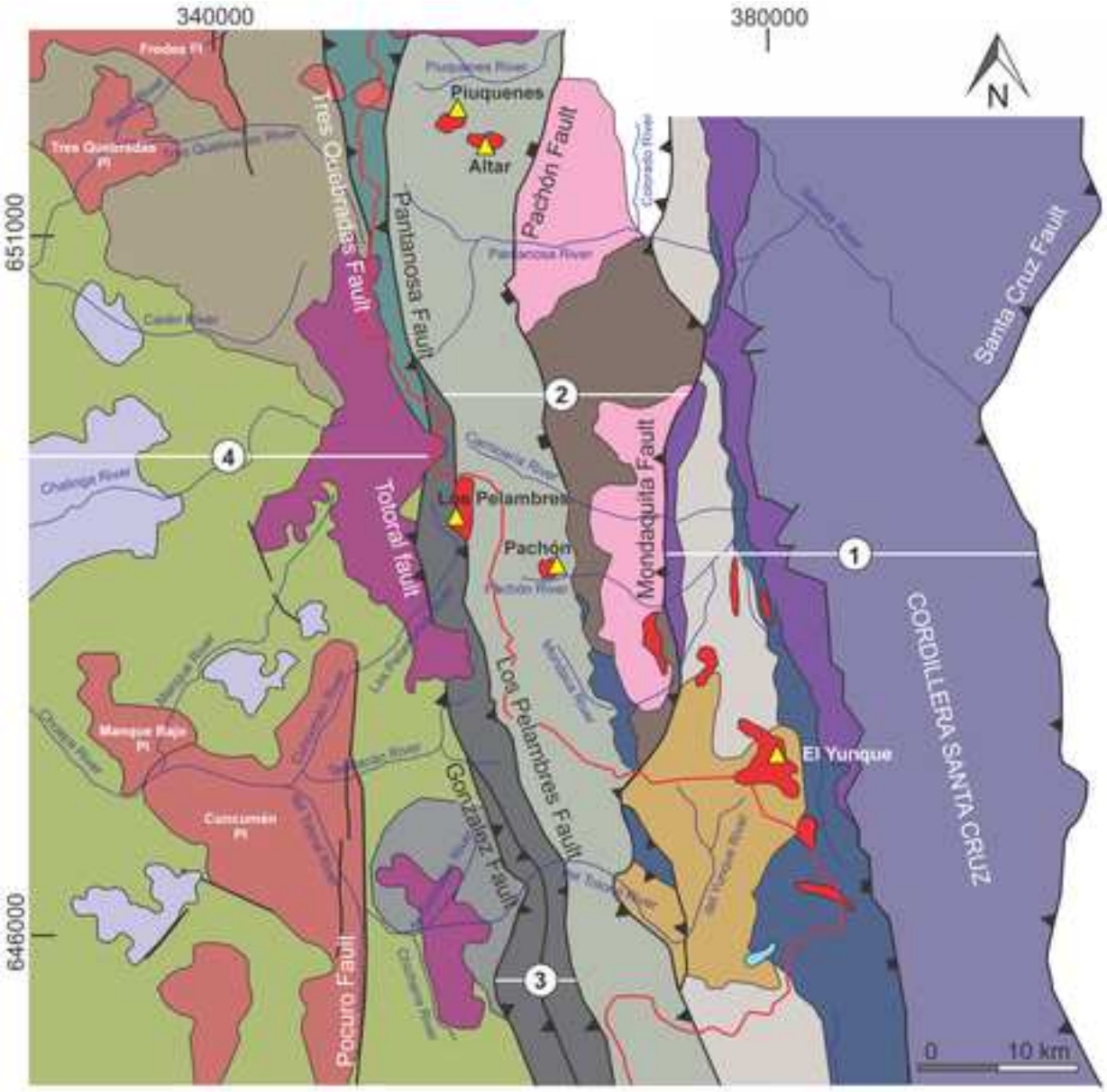

Stratified units

- Laguna del Pelado and Yunque volcanic units (Middle Miocene)
- Pachón Formation (Early Miocene)
- Mondaca Strata (Early Miocene)
- Río Chicharra Sequence (Upper Oligocene - Early Miocene)
- Los Pelambres Formation (Oligocene - Early Miocene)
- Paleocene volcanic units
- Cretaceous(?) volcanic and sedimentary strata
- Cretaceous volcano-sedimentary sequences
- Jurassic to Cretaceous sedimentary sequences (Neuquén Basin)
- Rancho de Lata Formation (Late Triassic)
- Middle Triassic volcanic rocks
- Permo-Triassic Choiyoi volcanic rocks and granitoids

Intrusive units

- Middle to Late Miocene intrusions (15-8 Ma)
- Early Miocene intrusions (24-14 Ma)
- Paleocene and Eocene intrusions (60-34 Ma)
- Late Cretaceous intrusions (74-65 Ma)
- Pico Los Sapos Batholith (Late Carboniferous - Early Permian)

- Chile-Argentina boundary
- River
- Thrust faults
- Inverted normal faults
- Lineaments
- ① Structural domains
- Porphyry deposit

Figure 3

Click here to access/download;Figure;Fig. 3.tif

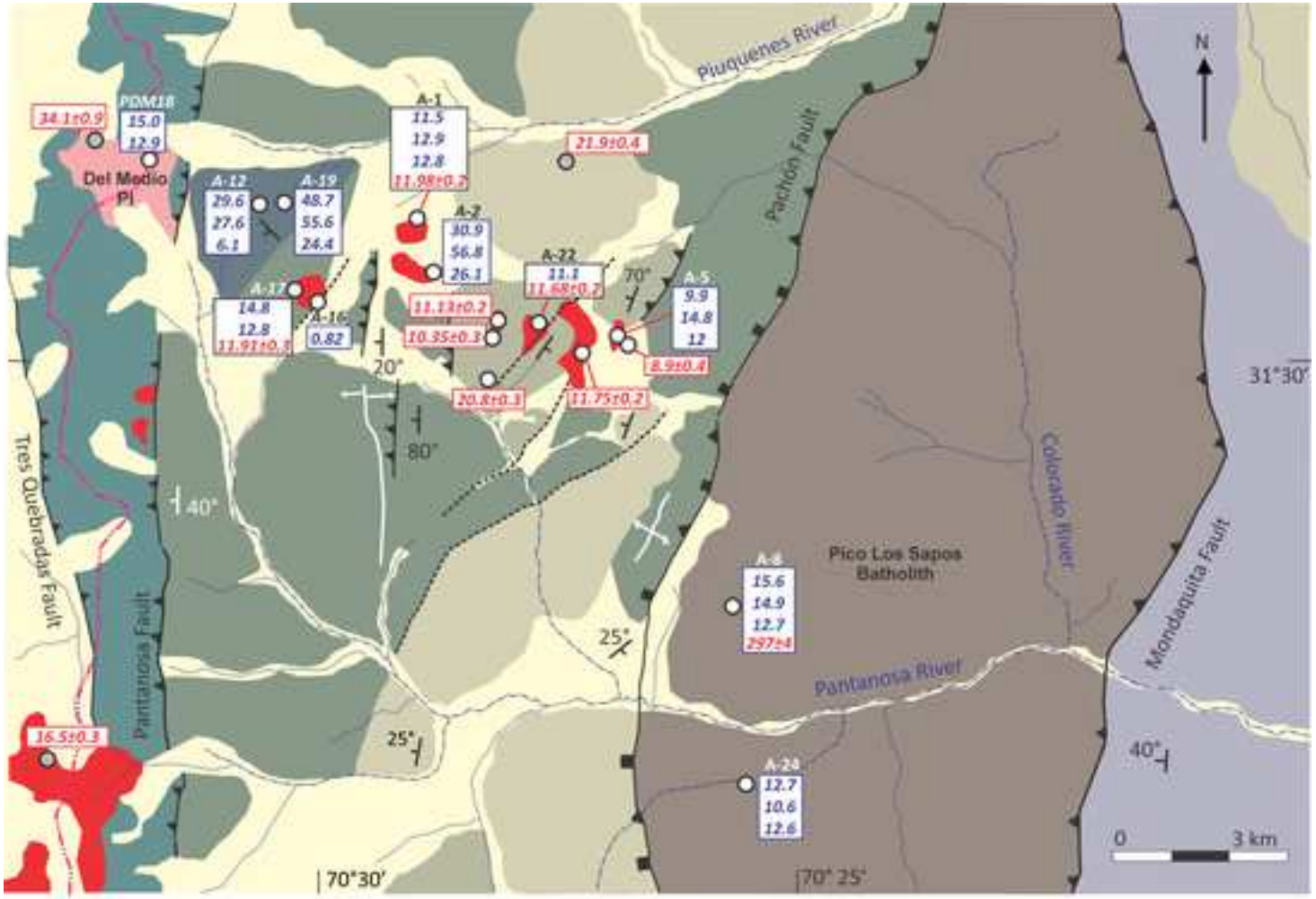

REFERENCES

U-Th/He
U-Pb

- U-Pb zircon Maydagán et al. (2011, 2012, 2014, 2017)
- U-Pb zircon Mpodozis (2016)
- Strike and dip of beds
- Ephemeral river
- Permanent river
- Lineaments
- Thrust faults
- Inverted normal faults
- Fold
- Chile-Argentina boundary

- Quaternary deposits
- Subvolcanic stocks (middle to late Miocene)
- Pyroclastic rocks (early Miocene)
- Andesite lavas (early Miocene)
- Volcano-sedimentary rocks (Miocene?)
- Tonalite (Eocene)
- Volcano-sedimentary rocks (Triassic-Jurassic?)
- Volcano-sedimentary rocks (Cretaceous?)
- Tonalite (Late Carboniferous)

Figure 4

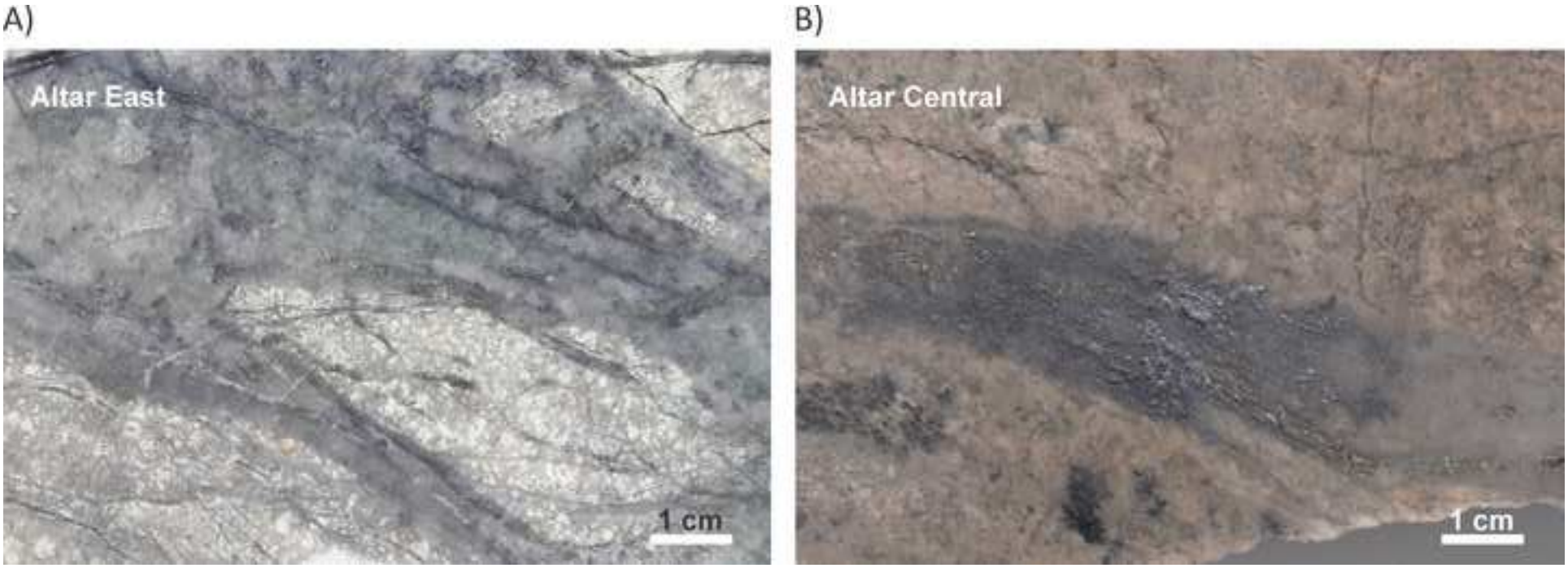

Figure 5

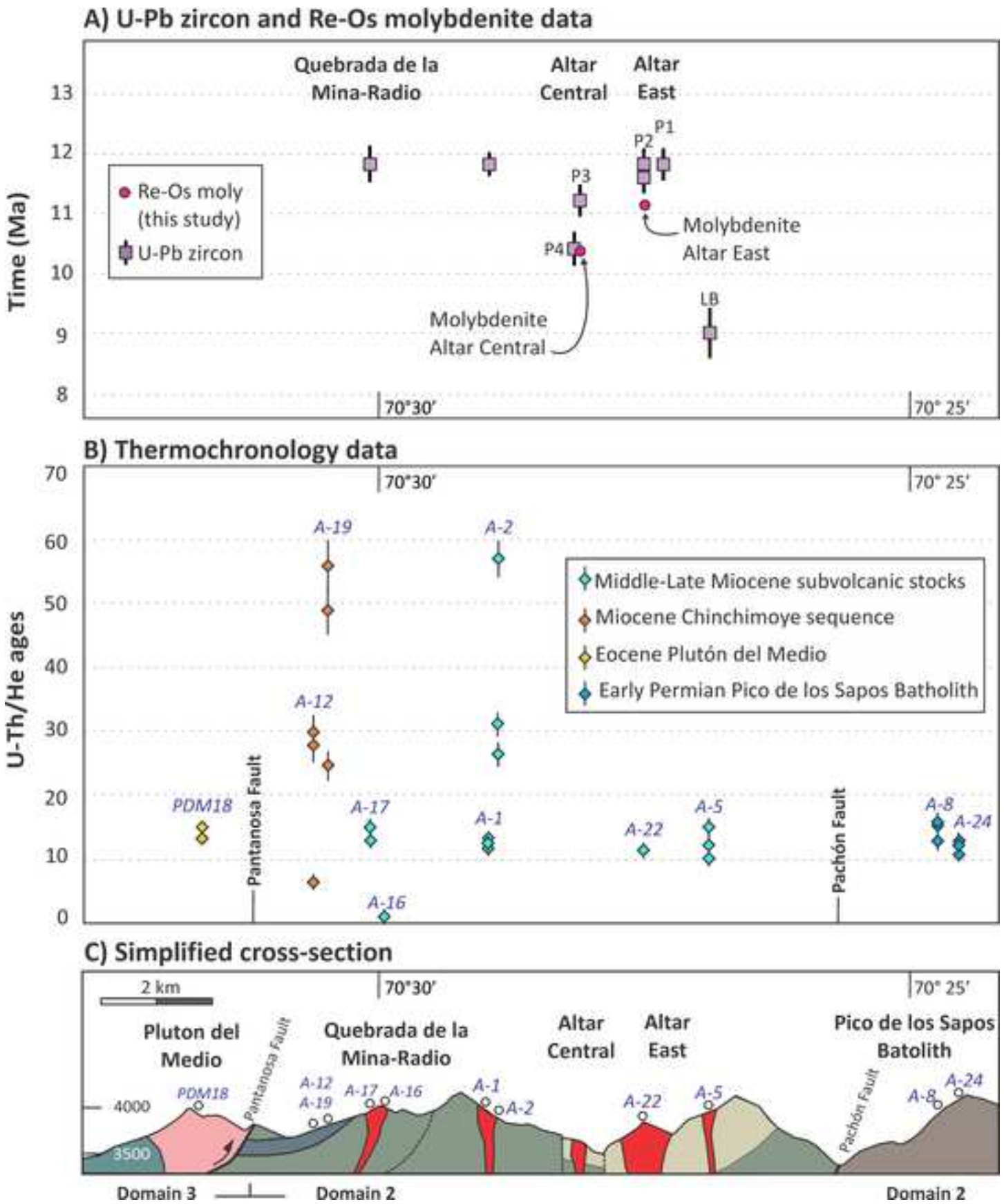

Figure 6

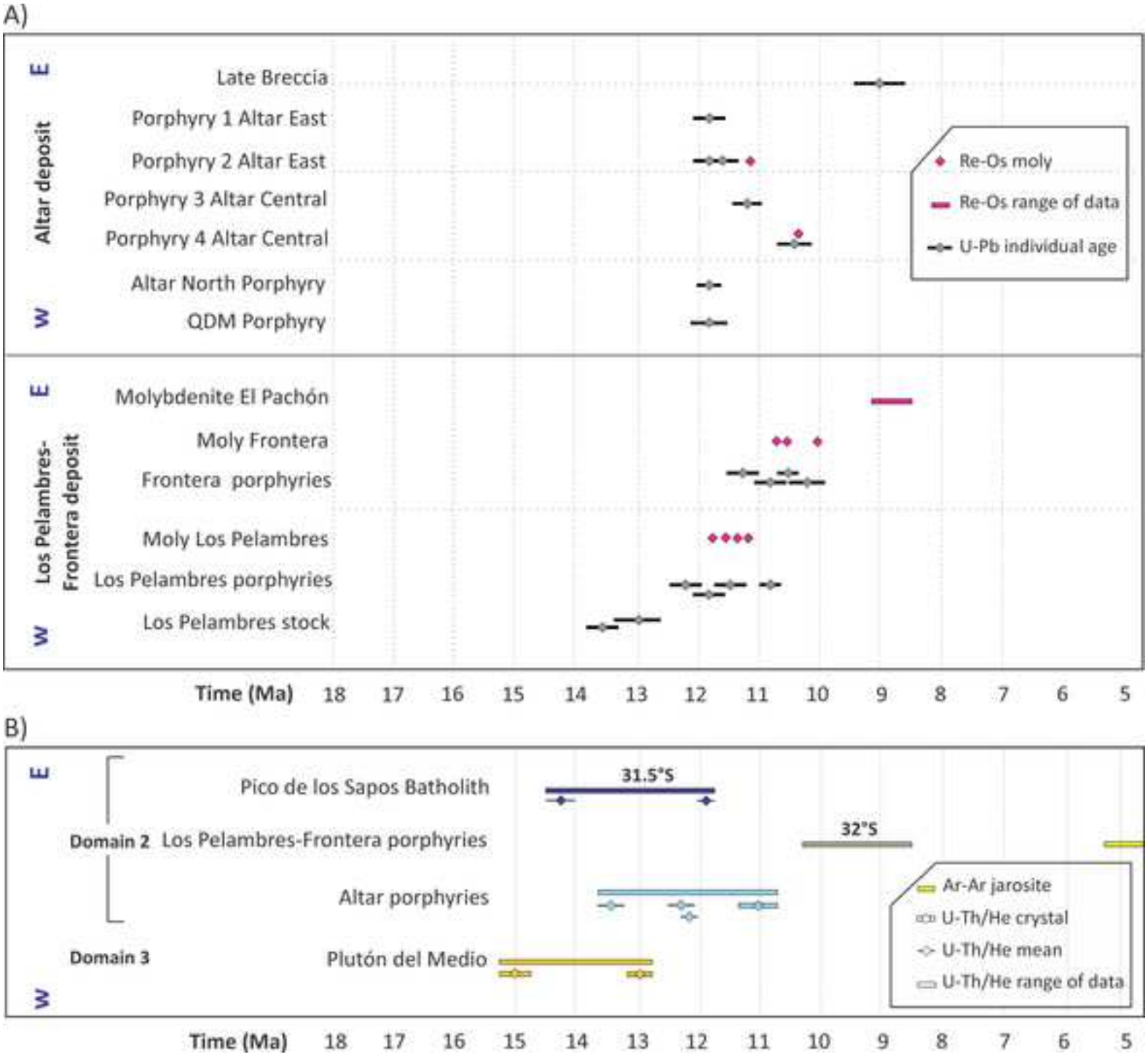

Figure 7

Click here to access/download;Figure;Fig. 7.tif

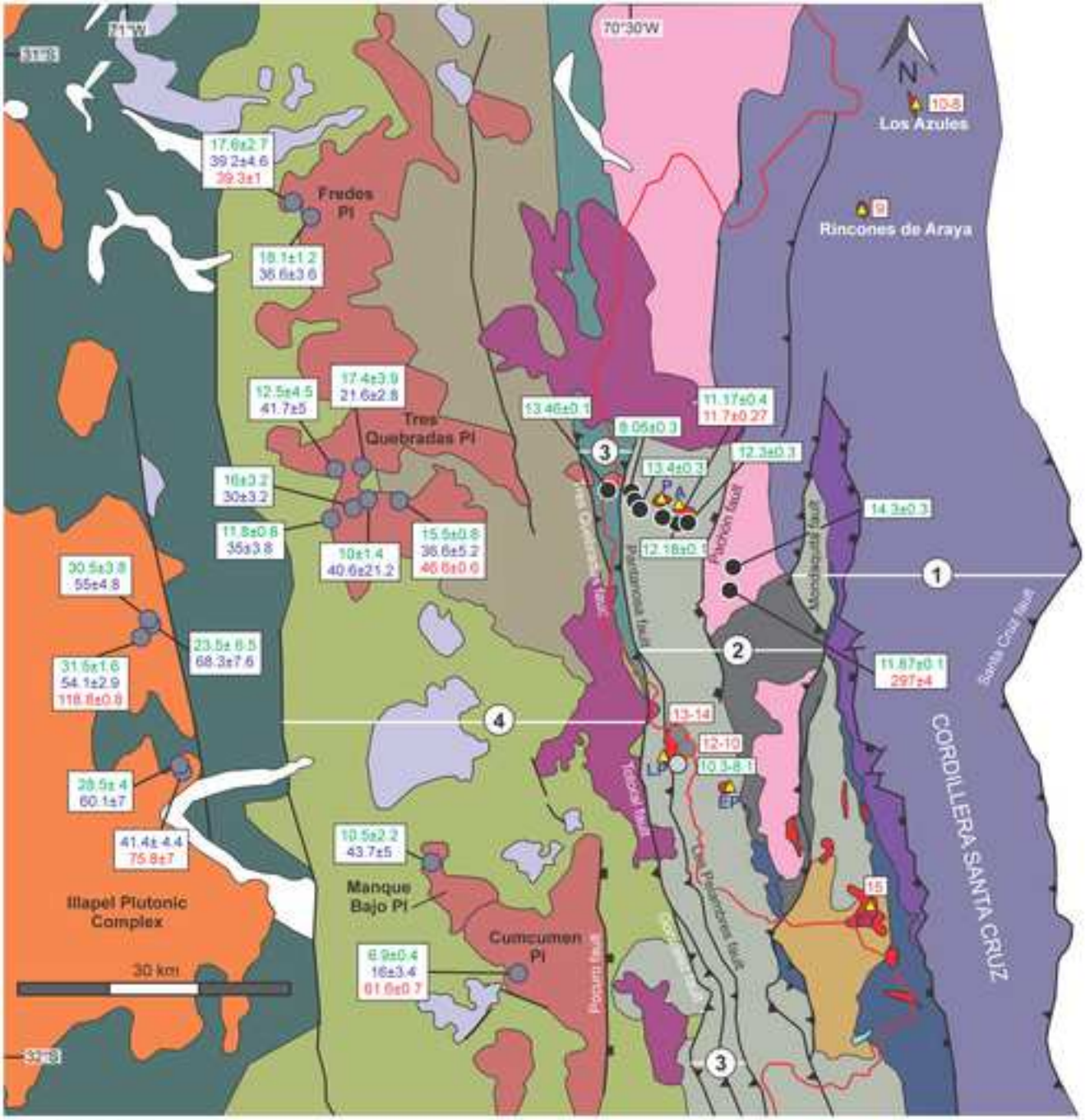

Stratified units

- Holocene sedimentary rocks
- Early Miocene volcanic rocks (19-18 Ma)
- Late Oligocene to Early Miocene volcanic rocks
- Paleocene volcanic rocks
- Cretaceous(?) volcanic and sedimentary strata
- Late Cretaceous volcano-sedimentary sequences
- Early to Middle Cretaceous volcano-sedimentary rocks
- Jurassic to Early Cretaceous sedimentary rocks
- Rancho de Lata Formation (Late Triassic)
- Middle Triassic volcanic rocks
- Permo-Triassic Choiyoi volcanic rocks and granitoids

Intrusive units

- Middle to Late Miocene intrusive rocks (15-8 Ma)
- Early Miocene intrusive rocks (24-14 Ma)
- Paleocene and Eocene intrusive rocks (60-34 Ma)
- Late Cretaceous intrusive rocks (74-65 Ma)
- Early to Middle Cretaceous intrusives
- Early Permian Granitoids

Geochronologic data:

- Rodriguez et al. (2018)
- Bertens et al. (2006)
- Perelló et al.(2012)
- This study

U-Th/He
FT apatite
U-Pb

- Thrust faults
- Inverted normal faults
- Lineaments
- Porphyry deposit
- Chile-Argentina boundary

ESM 1

Click here to access/download

Supplementary Material

ESM 1.pdf